



HINWEISE FÜR DIE ABFASSUNG DER 1. SEITE DER DIPLOMARBEIT

**DIPLOMARBEIT**

Netzwerktheoretische Betrachtungen der Unterschenkelmuskulatur  
Application of Circuit Theory on Modeling of Lower Leg Muscles

Thema

ausgeführt zum Zwecke der Erlangung des akademischen Grades eines Diplom-Ingenieurs  
unter der Leitung von

(Betreuer) Prof. Dipl.-Ing. Dr. Margit Gföhler  
Prof. Dipl.-Ing. Dr. Christian Peham  
Name  
E307  
Institutsnummer  
Konstruktionswissenschaften und Technische Logistik  
Institutsbezeichnung

eingereicht an der Technischen Universität Wien  
**Fakultät für Maschinenwesen und Betriebswissenschaften**

von

(Verfasser) Jakob Reuther, MSc.  
Name  
1127581  
Matrikelnummer  
Borschkegasse 5/18, 1090 Wien  
Anschrift

Wien, im \_\_\_\_\_

\_\_\_\_\_  
eigenhändige Unterschrift



TECHNISCHE  
UNIVERSITÄT  
WIEN  
Vienna University of Technology

Ich habe zur Kenntnis genommen, dass ich zur Drucklegung meiner Arbeit unter der Bezeichnung

## **D I P L O M A R B E I T**

nur mit Bewilligung der Prüfungskommission berechtigt bin.

Ich erkläre weiters an Eides statt, dass ich meine Diplomarbeit nach den anerkannten Grundsätzen für wissenschaftliche Abhandlungen selbständig ausgeführt habe und alle verwendeten Hilfsmittel, insbesondere die zugrunde gelegte Literatur genannt habe.

---

Datum

---

Unterschrift

## **Danksagung**

Ich möchte mich bei meinen Betreuern Dr. Margit Gföhler und Dr. Christian Peham für den Projektauftrag und die entgegen gebrachte Unterstützung bedanken. Zusätzlich möchte ich mich bei meiner Familie für die entgegengebrachte persönliche und finanzielle Unterstützung in den letzten Jahren bedanken, da ich mich so speziell auf das Studium konzentrieren konnte. Gerade meiner erst kürzlich verstorbenen Mutter gilt ein großer Dank - durch ihre journalistische Tätigkeit lernte ich schon in frühen Jahren viele unterschiedliche Themenbereiche kennen und konnte somit früh erkennen, dass ich im Bereich der Technik am Besten aufgehoben bin. Auch die Medizintechnik mit ihren vielen Facetten war immer wieder ein Teil ihrer Arbeit. Sie zeigte mir, dass man sich auch als Laie, in von außen komplex erscheinenden Gebieten, mit viel Eifer und Zielstrebigkeit in kurzer Zeit einarbeiten kann.

## Abstract

The aim of this work is to show that a mechanical Hill type muscle model of the human ankle can be represented and simulated with an electrical network equivalent by using the electromechanical analogies. The electrical circuit is built up with electrical elements (resistors, condensators, inductivities, current sources) according to the force-current analogy in mechanics (dampers, masses, springs, forces). The model includes the following muscles inducing a moment in the ankle joint: M. soleus, M. med. gastrocnemius, M. lat. gastrocnemius and M. tibialis anterior. Two control mechanisms are used to show up negative effects by not taking tendon properties into account. All electrical simulations were done with the software LTspice IV (1630 McCarthy Blvd., Milpitas, CA) in Windows Vista. Furthermore all simulations were carried out with OpenSim (3DGaitModel 2392) to compare the results with those of the electrical simulations.

The model follows the rules of ZAJAC [1989] and is able to accomplish forward dynamic tasks. With a given EMG stimulation signal as an input the model allows detailed examination of ankle angle, moment generation, muscle forces, tendon forces, fiber lengths, tendon lengths and fiber contraction velocities. Comparing the results with 3DGaitModel 2392 of OpenSim shows slight differences that can be referred to a variance in the force-length characteristics and a different moment of inertia. By changing muscle and inertial parameters the model can be used to simulate every type of joint, also non humans.

## Kurzfassung

Mit dieser Arbeit wird gezeigt, dass es möglich ist ein mechanisches Hill'sches Muskelmodell mit Hilfe des elektro-mechanischen Dualismus in ein elektrisches Modell überzuführen. Dabei werden mechanische Elemente (Dämpfer, Massen, Federn, Kräfte) gemäß der Kraft-Strom Analogie durch elektrische Elemente (Widerstände, Kondensatoren, Induktivitäten, Stromquellen) ersetzt. Es wurde ein Modell des menschlichen Sprunggelenks mit vier Muskeln (M. soleus, M. med. gastrocnemius, M. lat. Gastrocnemius, M. tibialis anterior) erzeugt. Zwei Steuerungsmechanismen zeigen wie sich die Nichtberücksichtigung der Sehneneigenschaften negativ auf die Ergebnisse auswirken. Die Simulationen wurden mit der Software LTspice IV (1630 McCarthy Blvd., Milpitas, CA) unter Windows Vista durchgeführt. Zur Überprüfung der Ergebnisse wurden die Simulationen mit OpenSim (3DGaitModel 2392) ebenfalls durchgeführt.

Das erzeugte elektrische Modell befolgt die Regeln von ZAJAC[1989] und ist somit in der Lage vorwärts-dynamische Analysen auszuführen. Mit einem EMG Signal können Gelenkwinkel, Momente, Muskelkräfte, Sehnenkräfte, Muskellängen, Sehnenlängen und Muskelkontraktionsgeschwindigkeiten ermittelt werden. Vergleiche mit den Ergebnissen von OpenSim zeigen geringe Abweichungen, die auf andere Kraft-Längen Eigenschaften sowie auf Unterschiede bei der Berechnung der Trägheitsmomente zurück zu führen sind. Das Modell kann durch verändern der Muskel- und Massenträgheitsparameter für jedes, auch nicht menschliche, Gelenk verwendet werden.

# Table of Contents

<b>1</b>	<b>Introduction</b>	<b>1</b>
<b>2</b>	<b>Anatomical structures used for the model</b>	<b>3</b>
2.1	Upper ankle joint . . . . .	3
2.2	Lower ankle joint . . . . .	4
2.2.1	Articulation subtalaris . . . . .	4
2.2.2	Articulation talocalcaneonavicularis . . . . .	4
2.3	Ligaments in the ankle joints . . . . .	4
2.4	Kinematics in the ankle joints . . . . .	4
2.5	Muscles acting at the ankle joints . . . . .	6
2.5.1	Dorsalflexors . . . . .	6
2.5.2	Plantarflexors . . . . .	6
<b>3</b>	<b>Muscle modelling</b>	<b>9</b>
3.1	Hierarchical architecture . . . . .	9
3.2	Contractile element properties . . . . .	10
3.2.1	Force-length properties . . . . .	11
3.2.2	Force-velocity properties . . . . .	13
3.2.3	Combining force-velocity and force-length properties . . . . .	16
3.3	Passive elements . . . . .	18
3.3.1	Passive element in parallel with the contractile element . . . . .	18
3.3.2	Passive element in series with the contractile element . . . . .	20
3.3.3	Angle of pennation . . . . .	22
3.4	Activation dynamics . . . . .	23
3.5	Model parameters . . . . .	26
3.5.1	Muscle parameters . . . . .	26
3.5.2	Skeletal parameters . . . . .	28
3.5.3	Movement definitions . . . . .	28
<b>4</b>	<b>Electromechanical analogies</b>	<b>29</b>
4.1	Example for converting a mechanical system into an electrical circuit . . . . .	30
4.2	Hill's electrical equivalent . . . . .	32

<b>5 Model control</b>	<b>33</b>
5.1 Musculo-Tendon-control . . . . .	33
5.2 Muscle-fiber-length-control . . . . .	35
5.3 Differences between electrical simulation and numerical simulations . . . . .	36
<b>6 Results</b>	<b>38</b>
6.1 Simulation case 1 . . . . .	38
6.2 Simulation case 2 . . . . .	43
<b>7 Discussion</b>	<b>48</b>
7.1 Simulation case 1 . . . . .	48
7.2 Simulation case 2 . . . . .	49
<b>8 Conclusion</b>	<b>52</b>
<b>References</b>	<b>54</b>

# 1 Introduction

Muscle modeling started with HILL [1938] and HUXLEY [1957] and nowadays simulations refer basically on the musculo-tendon-model of ZAJAC [1989]. Till the late 1980's the computers did not have the capacity to compute a larger model (e.g. to run a forward dynamic problem) but since the computational capacity has risen with large steps many different simulations with muscle models have been carried out. These computer models help us to understand biomechanical interactions in living organisms. They help us to understand the different structures responsible for our movements: muscle, tendon, cartilage and bone. Simulations can figure out the forces in muscles, tendons and joints. E.g. this knowledge is used to design new implants or surgery techniques in orthopedics. Sports simulations are used to understand and improve specific movements like running or jumping. Furthermore simulations can be used to determine effects of an aging muscle (THELEN [2003]) which will be a major issue in our future because of rising average population age.

The major problem of these models is the limited amount of experimental data they are based on. ARNOLD et al. [2010] based a model for the lower limb on the work of WARD et al. [2009] including 21 cadavers. Before muscle models were even based on a smaller amount.

## **Aim of work**

Normally muscle models are programmed numerically. In this work I tried to perform an electrical simulation by building an electrical network which has the same properties as the the musculo-tendon model of ZAJAC [1989]. The reason for using an electrical simulated model is the flexibility - it can be used for every different joint (also non human) and a variable number of muscles included in the simulation. Only the individual muscle and joint parameters have to be adapted to run a simulation. With an electrical simulation software (in this work I used LTspice IV (1630 McCarthy Blvd., Milpitas, CA)) the electrical quantities voltage and current can easily be observed at every point of the network. These electrical quantities represent the mechanical quantities and therefore the model can also be used by people who are not so familiar with mechanics and informatics.

In this work I show two different possibilities of controlling a muscle. One with the musculo-tendon-unit of ZAJAC [1989] and the second approach uses only the muscle-fiber-length and does not consider the tendon with it's properties. My model allows for a given stimulation pattern (e.g. EMG data can be used) detailed examination of moment generation, muscle force, tendon force, fiber length, tendon length and fiber contraction velocities in the human ankle joint. Furthermore the model can be used to perform a forward dynamic simulation of the ankle's movement.

In future this work should be extended to a model of a horse spine to simulate moments and forces on vertebral joints. As a basis the horse's muscles and joints have to be examined to define the individual muscle and joint parameters. In this work all human muscle parameters are taken from ARNOLD et al. [2010]'s model. The results from the horse's spine analysis could be used and transmitted on the human body. This could maybe show some unknown effects and linkages.

## 2 Anatomical structures used for the model

The ankle joint can be divided into two joints:

- upper ankle joint
- lower ankle joint

In the following paragraphs the articulating bones, the ligaments, the acting muscles and the possible kinematics will be analyzed.

### 2.1 Upper ankle joint

The human ankle joint combines the structures of the lower limb and the foot. In the upper ankle joint (*articulatio talocruralis*) the distal ends of the two bones from the lower limb (tibia and fibula) articulate with the talus (figure 2.1). Both - malleolus medialis and lateralis - have a hyaline cartilage on their inside. The distal parts of tibia and fibula are connected by the syndesmosis tibiofibularis. This structure consists mostly of collagen and is not very ductile.

The talus is the most important part between the upper and lower ankle joint. Like the inner parts of the malleols the talus has three areas covered with hyaline cartilage. According to SCHMITZ [1985] the thickness of the cartilage ranges from 0.3 - 1.3mm. On the proximal part of the corpus tali the articulating part is called *trochlea tali*. The area articulates with the two malleols in the upper ankle joint. In an approximation the curvature can be assumed to be circular [KUMMER, 2005].

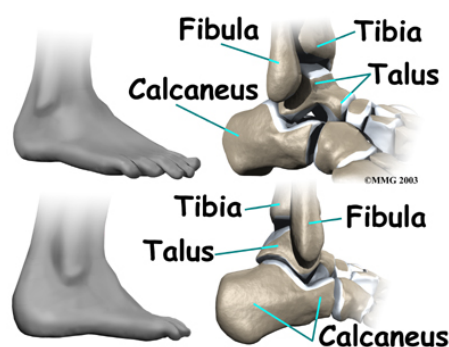


Figure 2.1: Articulating bones in the ankle joints [eor, 2013]

## 2.2 Lower ankle joint

The lower ankle joint - articulatio talotarsalis - is built up by two separate joints which are a functional unit:

- articulatio subtalaris
- articulatio talocalcaneonavicularis

The major bone participating in the lower ankle joint is the calcaneus. It articulates with the talus and the cuboid. On the posterior part of the corpus calcanei is the tuber calcanei. At this point the Achilles tendon inserts. Due to this fact this joint represents a major area for plantarflexion as well as for dorsalflexion [KUMMER, 2005].

### 2.2.1 Articulation subtalaris

The articulatio subtalaris represents the posterior part of the lower ankle joint. In this joint which has a separate articular capsule act the facies articularis calcanea posterior of the talus and the facies articularis talaris posterior of the calcaneus. The articulating area has the form of a cylindrical curvature. In front of this area exists a channel called sinus tarsi [KUMMER, 2005].

### 2.2.2 Articulation talocalcaneonavicularis

This joint represents the anterior part of the lower ankle joint. Like the articulatio subtalaris it has a separate articular capsule. Caput tali articulates with the facies articulares talaris anterior and medial of the calcaneus as well as with the posterior part of the naviculare [KUMMER, 2005].

## 2.3 Ligaments in the ankle joints

The strongest ligaments are found in the upper ankle joint. The lig. deltoideum connects the malleolus medialis with the naviculare, talus and calcaneus (figure 2.2). On the lateral upper ankle joint the lig. talofibulare anterius acts as a stabilizing structure. The lig. calcaneofibulare acts in the upper and lower ankle joint, lig. talocalcaneare laterale only in the lower ankle joint [KUMMER, 2005].

## 2.4 Kinematics in the ankle joints

Both joints have a separate axes which collide in the sinus tarsi. The upper as well as the lower ankle joint both have only one degree of motion. Putting the foot plantar on the ground the axis in the upper ankle joint is nearly horizontal in the frontal plane. The axis in the lower ankle joint runs from plantar to dorsal. Both joints interact and work like a cardan joint.

As no muscle directly acts on the talus always both ankle joints (upper and lower) are used to

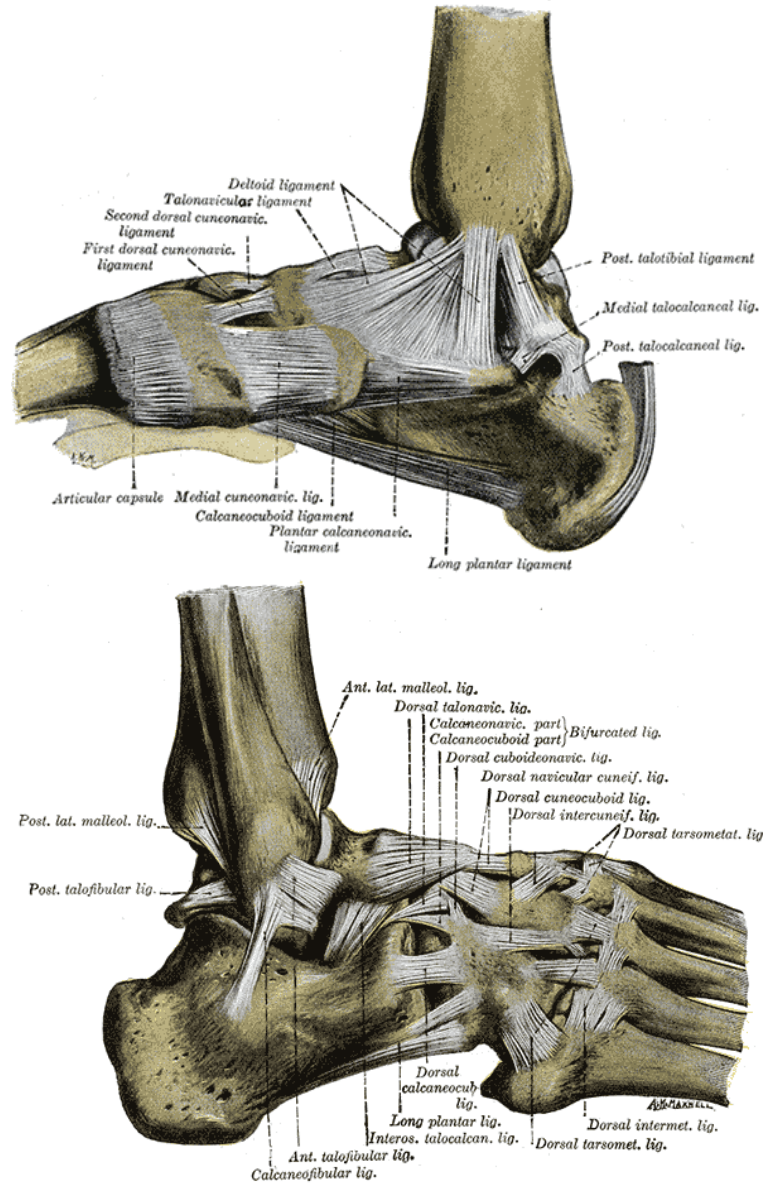


Figure 2.2: Medial (upper) and lateral (lower) ligaments in the ankle joint [GRAY, 1918]

perform a motion. However by combining specific muscle forces an isolated motion in one of the joints is also possible. In the upper ankle joint flexion and extension (plantar- and dorsalflexion) is performed. As mentioned before, pure extension can be performed only when the lower ankle joint is stabilized by muscular forces. In the lower ankle joint pronation and supination is carried out. During pronation the medial foot is lowered and the tip of the foot is moved outward. During supination it behaves in the opposite way: the medial foot is lifted and the tip of the foot moves inward. These motions can also be performed isolated (no movement in the upper ankle joint) when stabilizing the upper joint by muscular forces. In most cases both axes are used for a combination of these two movements (extension + pro- or supination) [KUMMER, 2005].

## 2.5 Muscles acting at the ankle joints

In the ankle two major groups of muscles occur:

- Extensors of the foot (Dorsalflexors)
- Flexors of the foot (Plantarflexors)

As a third group exist the Mm. peronei longus and brevis. Both originate at the fibula and insert at the metatarsus. These muscles act as pronators in the lower ankle joint and as plantarflexors in the upper ankle joint. They play a major role in preserving the arch of the foot [KUMMER, 2005].

### 2.5.1 Dorsalflexors

This muscle group originates on the anterior part of the lower leg and inserts either at the tarsal bones or at the toes (figure 2.3). The tibialis anterior can perform the dorsalflexion and supination. Mm. extensores digitorum longus and hallucis longus do a pronation beside the dorsalflexion. All tendons reaching from the lower limb to the foot are fixed to the skeleton by the retinacula mm. extensorum superius and inferius [KUMMER, 2005].

### 2.5.2 Plantarflexors

Muscles of this group originate at the dorsal part of the lower leg (figure 2.4). All of them, except the triceps surae which inserts at the posterior part of the calcaneus (tuber calcanei), insert at the planta pedis - either at the tarsal bones or at the toes. M. triceps surae consists of m. soleus and the m. gastrocnemius medialis and lateralis. The two gastrocnemial heads act both at the knee and in the ankle joint - M. soleus only at the ankle joint. All three together act over the Achilles tendon as a strong plantarflexor as well as a supinator. The other plantarflexors are Mm. tibialis posterior, flexor digitorum longus and flexor hallucis longus. All of them act also as supinators because all their tendons act medial of the axis in the lower ankle joint. Like the tendons of the dorsalflexors also those of the plantarflexors are fixed by retinacula mm. flexorum superius and inferius.



Figure 2.3: Muscles in a right ankle joint from dorso-lateral. 1 Retinaculum extensorum superius, 2 Retinaculum extensorum inferius (Lig. cruciforme), 3 Mm. peronei (superficial the tendon of M. peroneus longus) and behind the Achilles tendon of M. triceps surae, 4 M. extensor digitorum longus, 5 M. extensor hallucis longus, 6 M. tibialis anterior [KUMMER, 2005]

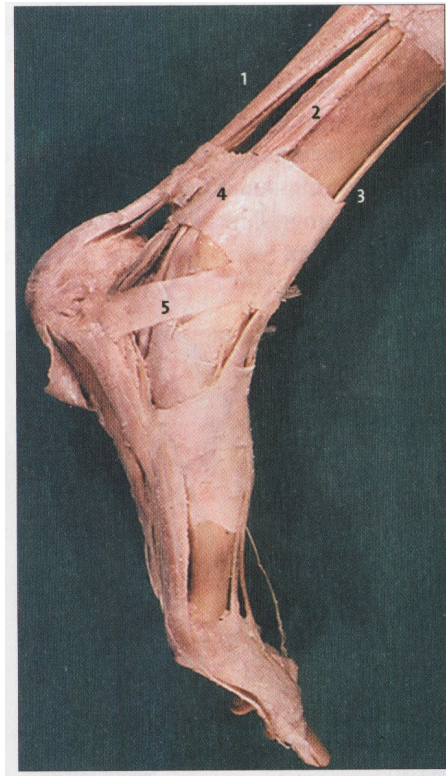


Figure 2.4: Muscles in a left ankle joint from medial. 1 M. triceps surae 2 M. flexor digitorum longus, 3 M. tibialis anterior, 4 Retinaculum flexorum superius, 5 Retinaculum flexorum inferius [KUMMER, 2005]

## 3 Muscle modelling

A muscle is an organ that extends from a distal muscle-tendon junction to a proximal one. The available force to produce a joint moment depends on muscle architecture, the velocity of the contraction and on the current length of the muscle. The torque is always produced by an interaction of muscle fibers and the corresponding tendon. Modeling the tendon as a pure rigid link is not possible because of its non-linear property. Beside the major function of producing force and hence movements, muscles produce a significant amount of heat to regulate the body temperature. Muscles are able to perform tasks with a high precision like handwriting as well as tasks needing a high amount of energy like sprinting [EPSTEIN and HERZOG, 1998, p. 3].

### 3.1 Hierarchical architecture

The contractile element consists of actin and myosin filaments which reside in a sarcomere overlapping each other. A muscle fiber is a cell with a very sensible membrane, called sarcolemma. In a single muscle fiber many parallel myofibrils, which consist of sarcomeres arranged in parallel, act together. Many muscle fibers in parallel form a muscle fiber bundle or fascicle (figure 3.1).

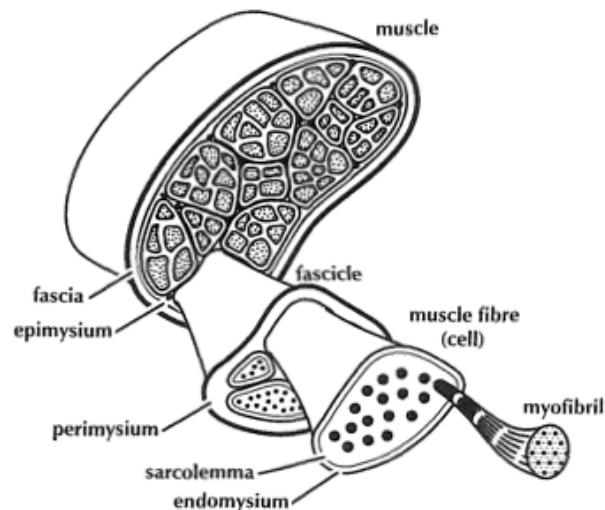


Figure 3.1: Hierarchical structure of muscles [EPSTEIN and HERZOG, 1998, p. 4].

The interactions of the filaments in the sarcomere are responsible for the production of force which is transmitted to the tendon. At both ends of an sarcomere the Z-lines separate the sarcomere from the next ones (figure 3.2). The thick filament myosin is in the center of the sarcomere. On the

outer parts of the myosin filaments exist heads which act as binding sites for the actin filaments. If an actin filament binds to a head of the myosin it gets pulled towards the center of the sarcomere (contracting muscle). These connections between the two filament types are called cross-bridges.

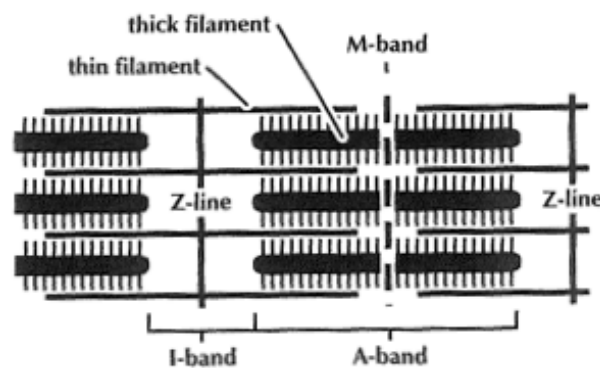


Figure 3.2: Sarcomere - the basic contractile unit of a muscle [EPSTEIN and HERZOG, 1998, p. 4].

The distance between the cross-bridges on the myosin is 14.3nm and they are always rotated by a  $60^\circ$  rotation (figure 3.3). The distance between two thick filaments is 42nm and each myosin filament is surrounded by six actin filaments - like a perfect hexagon (figure 3.4).

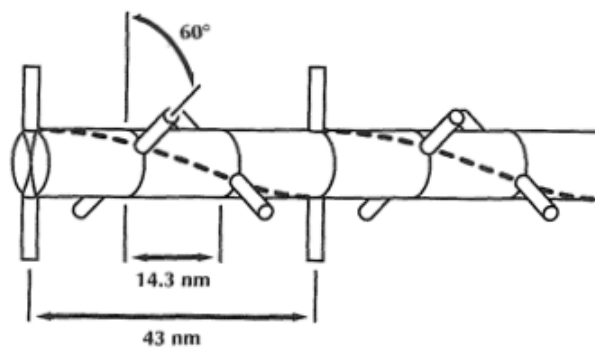


Figure 3.3: Arrangement of the cross-bridges in the thick filament [EPSTEIN and HERZOG, 1998, p. 6].

## 3.2 Contractile element properties

For modeling a muscle a variety of important aspects have to be considered. Using a Hill-type model (HILL [1938]) three major components have to be described: the contractile force generating element and two elastic components - one for the tendon and another one for the connective tissue structure surrounding the muscle fibers [EPSTEIN and HERZOG, 1998, p. 23].

A muscular structure can be simplified by a straight line model (EPSTEIN and HERZOG [1998, p. 24]). These models have in the simplest form either a parallel-fibered or a pennate-fibered

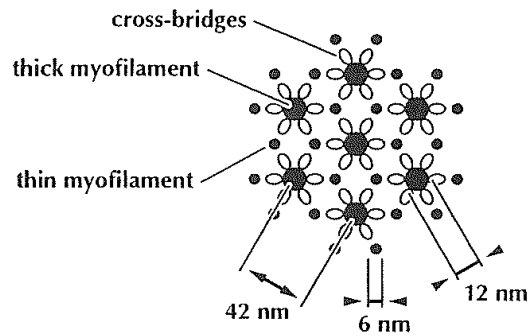


Figure 3.4: Arrangement of thick and thin filaments in a cross-sectional view in the overlapping zone [EPSTEIN and HERZOG, 1998, p. 7].

contractile element. Pennate muscles have the fibers aligned in a distinct angle relative to the line of the muscle. The different muscle shapes occur because of a variety of functional tasks which have to be fulfilled in agonistic muscle groups. According to the number of fiber orientations in a muscle there exist 3 different categories. A unipennate muscle has fibers aligned in one direction. Two distinct fiber directions indicate a bipennate muscle and a multipennate muscle exceeds two directions.

The behaviour of a contractile element is described with a force-length and a force-velocity property.

### 3.2.1 Force-length properties

BLIX [1894] has already mentioned the force-length dependency long time ago. Over the years force-length properties have been derived for sarcomeres (GORDON et al. [1966]), for isolated fibers (TER KEURS et al. [1978]) and for entire muscles (GOSLOW and VAN DE GRAAF [1982], HERZOG et al. [1992], HERZOG and TER KEURS [1988]). For modeling a whole muscle the properties of a sarcomere are not as relevant as the properties for a entire muscle.

The simple case of a symmetric force-length relation was described by WOITTIEZ et al. [1984]. It needs two parameters: the maximum isometric peak force  $F_0$  and the working range  $L$ . The maximal isometric force a muscle can generate is a function of the physiological cross-sectional area (PCSA) (EPSTEIN and HERZOG [1998, p. 26]):

$$PCSA = \frac{MuscleVolume}{FiberLength} \quad (3.1)$$

The optimal sarcomere length for humans is at  $2.7\mu\text{m}$  (WALKER and SCHRODT [1973]). The PCSA is the sum of cross-sectional areas of all fibers arranged in parallel. The peak isometric force is calculated by multiplying PCSA with the maximum muscle stress  $k$ :

$$F = k * PCSA \quad (3.2)$$

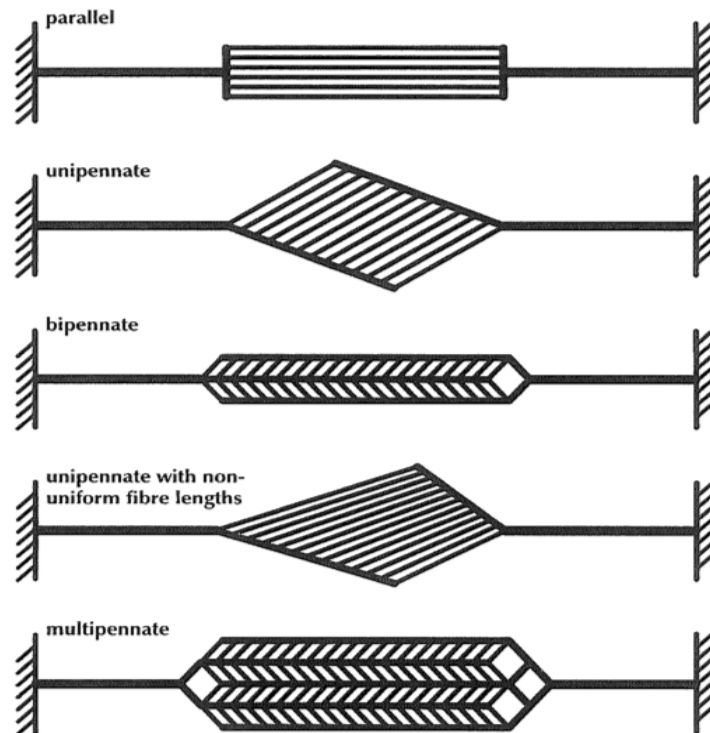


Figure 3.5: Straight line models for parallel and pennate fibered muscles [EPSTEIN and HERZOG, 1998, p. 25].

The  $k$ -values differ in the literature between  $9.8\text{N/cm}^2$  (WEBER and WEBER [1836]) to  $147\text{N/cm}^2$  (PEDOTTI et al. [1978]). The simple symmetric force-length relation is described with following formula (figure 3.6):

$$F(L) = -6.25 \left( \frac{L}{L_0} \right)^2 + 12.5 \left( \frac{L}{L_0} \right) - 5.25 \quad (3.3)$$

$L_0$  notes the optimal fiber length at which the muscle can produce the maximum force;  $L$  is the current fiber length and  $F$  the normalized current force. The force-length relation shown with equation 3.3 has a normalized working range from 0.6 to 1.4. Studies from ZAJAC [1989] show a working range from 0.5 to 1.5. DELP [1990] uses a working range from 0.4 to 1.6 and VAN SOEST [1992] is mentioning a working range from 0.44 to 1.56. Equation 3.4 from GUENTHER [1997] gives the possibility to use different working ranges by defining the parameter *width*.  $F$  becomes 1 at the optimal fiber length  $L_0$  and 0 if the interval is outside  $(1 - \text{width}) \leq L/L_0 \leq (1 + \text{width})$ .

$$F(L) = -\frac{1}{\text{width}^2} * \left( \frac{L}{L_0} \right)^2 + \frac{2}{\text{width}^2} \left( \frac{L}{L_0} \right) - \frac{1}{\text{width}^2} + 1 \quad (3.4)$$

Modeling a joint needs the force-length characteristics of all involved muscles. The muscles can have similar force-length properties resulting in a high peak force because all muscles reach the

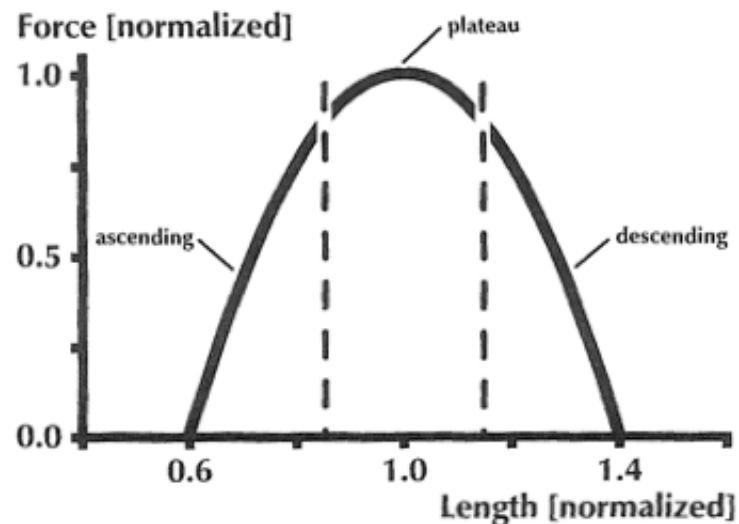


Figure 3.6: Normalized force-length relation of mammalian skeletal muscle obeying equation 3.3 [EPSTEIN and HERZOG, 1998, p. 29].

maximum force at the same joint angle (Figure 3.7a). This is an ideal case which normally not occurs in nature because all muscles would connect the same origin and onset points with the same muscle architecture. Different force-length properties result in a lower maximum force but in a higher working range (Figure 3.7b). *"For human subjects who use muscles primarily for normal everyday tasks such as locomotion, force-length properties across subjects are probably similar"*, says EPSTEIN and HERZOG [1998, p. 32]. But HERZOG et al. [1991] could show that a specific training can adapt the muscles force-length properties. Runners who use their rectus femoris at longer fiber lengths than cyclists were stronger at longer fiber lengths. It is assumed that the reason is an increase of sarcomeres in series. In all my simulations I use equation 3.4 from GUENTHER [1997] with a width of 0.6.

### 3.2.2 Force-velocity properties

*"The force-velocity relation describes the maximal, steady-state force of a muscle as a function of its rate of change in length"*, EPSTEIN and HERZOG [1998, p. 36]. HILL [1938] was the first who described the force-velocity relation for **shortening** muscles at optimal length (equation 3.5). With increasing shortening velocity, the maximal force the muscle can produce, decreases. At the maximum shortening velocity  $v_0$  the muscle can not sustain any tension 3.8. On the other hand when a muscle gets stretched at a given speed, the force exceeds the maximal isometric force. The maximum values of the forces depend on the experiment (isokinetic(EDMAN et al. [1978]) or isotonic(KATZ [1939])). EPSTEIN and HERZOG [1998, p. 38] assume that the maximum force

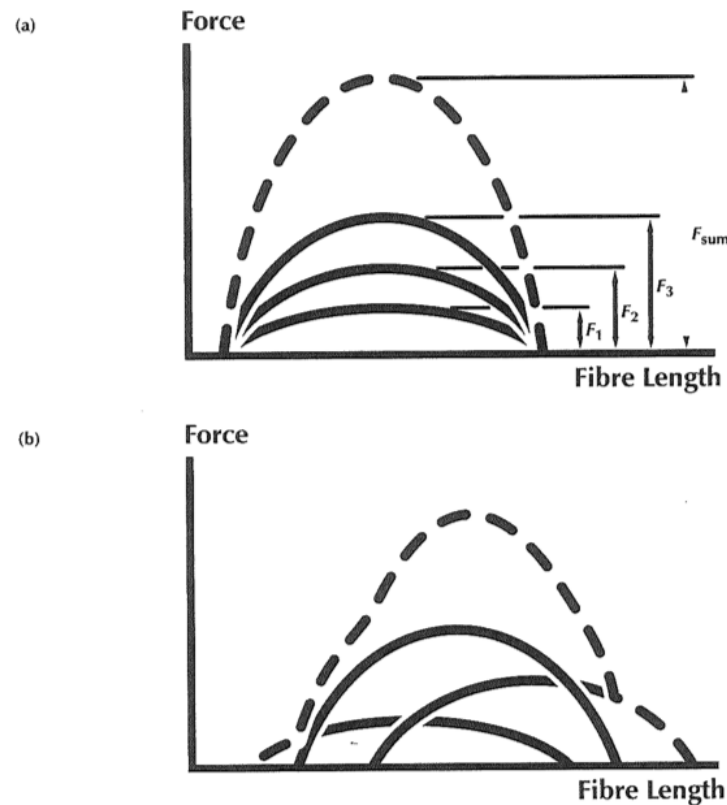


Figure 3.7: Total force-length relation (dashed line) of a synergistic group of muscles with (a) similar force-length properties of the individual muscles (solid lines), and (b) with different force-length properties of the individual muscles [EPSTEIN and HERZOG, 1998, p. 33].

for a stretched muscle has an asymptotic value of  $2F_0$ . ZAJAC [1989] states a value of  $1.8F_0$ .

$$(F + a)(v + b) = (F_0 + a)b \quad (3.5)$$

$F_0$  is the maximal isometric force at optimal contractile element length;  $F$  can be calculated for a certain  $v$  or viceversa;  $a$  and  $b$  are constants with units of force and velocity. To calculate  $F$  the constants have to be known. Therefore the equation is rewritten for a contraction with maximal velocity  $v_0$  - the force becomes zero:

$$F_0 b = a v_0 \quad (3.6)$$

HILL [1970] found out, that  $a/F_0$  and  $b/v_0$  approximately equal to 0.25 for human fast twitch fibers at 37°C. FAULKNER et al. [1980] and FAULKNER et al. [1986] determined the same value of 0.25 for fast twitch fibers and 0.15 for slow twitch fibers. The maximal isometric force is nearly the same for fast and slow twitch fibers, but the maximal shortening velocity differs by a factor of 3 or 4.

However, these numbers show that it is very important to know about the fiber-type distribution when modeling a muscle. All muscles are a mixture of slow- and fast-twitch fibers and an exact value for the distribution can be determined only with a biopsy. HILL [1938] found that the regular force-velocity equation (equation 3.5) fitted the mixed-fibered muscle well, except at forces below 5% of  $F_0$ . Here the real values were much higher than the predicted ones. The major effect of slow- and fast-twitch fibers can be seen when looking at the power production.

$$P = F \cdot v \quad (3.7)$$

$F$  and  $v$  are vectors multiplied with the dot product. The power output of a fast-twitched muscle is always higher than that of a slow-twitched one (figure 3.8).

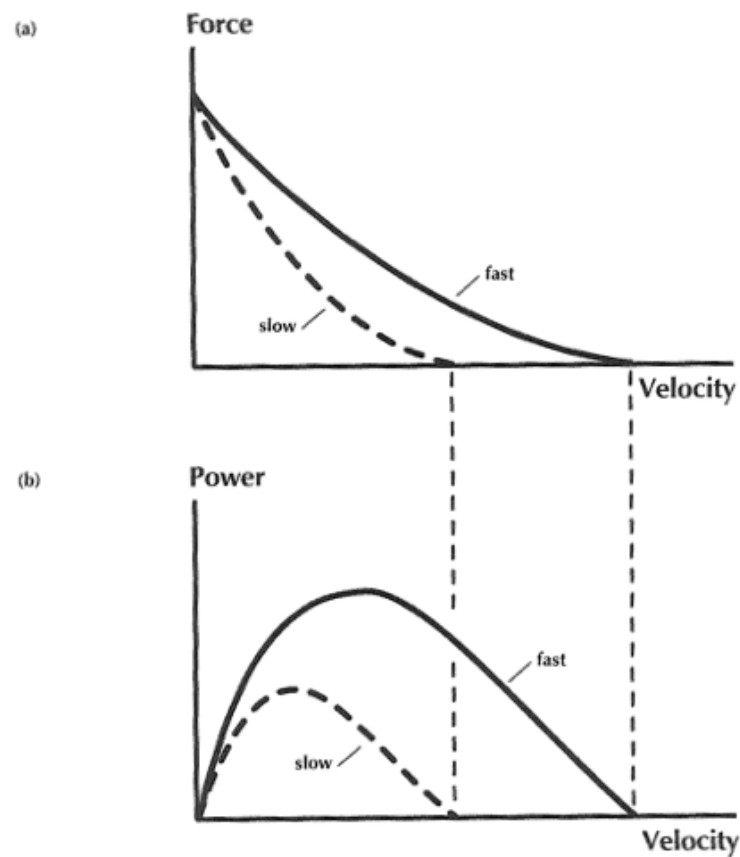


Figure 3.8: (a) force-velocity properties and (b) power-velocity properties of fast- and slow-twitched fibers [EPSTEIN and HERZOG, 1998, p. 40].

THELEN et al. [2003] describes the force velocity relationship with a sigmoidal:

$$f(v) = 1.8 - \frac{1.8}{1.0 + e^{\frac{0.04 - \frac{v}{v_0}}{0.18}}} \quad (3.8)$$

In this equation the ratio of fast- and slow-twitched fibers is described with the maximum contraction velocity  $v_0$ . The value 1.8 describes the maximum normalized force during an eccentric contraction  $F = 1.8F_0$  (figure 3.9).

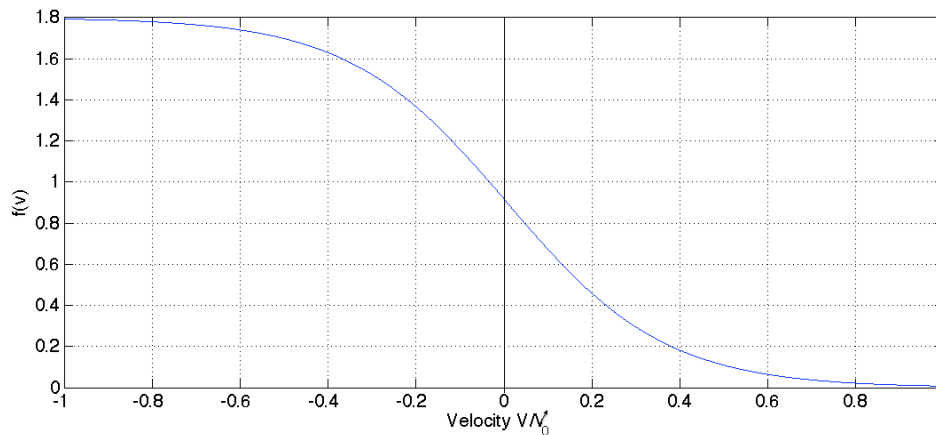


Figure 3.9: Sigmoidal force-velocity-relation from THELEN et al. [2003].

### 3.2.3 Combining force-velocity and force-length properties

Till now I explained how the force-velocity and force-length properties are described separately. Modeling a muscle needs the combination of these two factors. Therefore the force-velocity relation of HILL [1938] is multiplied with the normalized force-length relation of equation 3.3:

$$F = \frac{F_0 b - av}{b + v} * F(l) \quad (3.9)$$

EDMAN [1979] showed that equation 3.9 is true for contractile element lengths ranging from  $1.65\mu\text{m}$  to  $2.70\mu\text{m}$ . In figure 3.10 it can be seen that the maximum shortening velocity nearly remains constant for the mentioned sarcomere lengths. Therefore a different representation of the force-length-velocity relation (equation 3.9) is required for sarcomere lengths outside  $1.65\text{-}2.70\mu\text{m}$ .

GUENTHER [1997] formulated the equation of HILL [1938] in a different way to combine the force-length relation (equation 3.4) and the force-velocity relation (equation 3.5):

$$F = \frac{-q * F_0 * (A_{\text{rel}} * v + B_{\text{rel}} * F(L) * \text{Factor}(q) * L_0)}{v - B_{\text{rel}} * \text{Factor}(q) * L_0} \quad (3.10)$$

$F(L)$  is the isometric force in the force-length relation (equation 3.4).  $L_0$  is the optimal fiber length where the muscle can produce the maximum force  $F_0$ .  $q$  is the activation of the muscle (chapter 3.4). Figure 3.11 shows the force-velocity curve for different activation levels  $q$ . According to VAN SOEST [1992]  $\text{Factor}(q) = 1$  for  $q > 0.3$  and in other cases  $\text{Factor}(q) = q/0.3$ . This

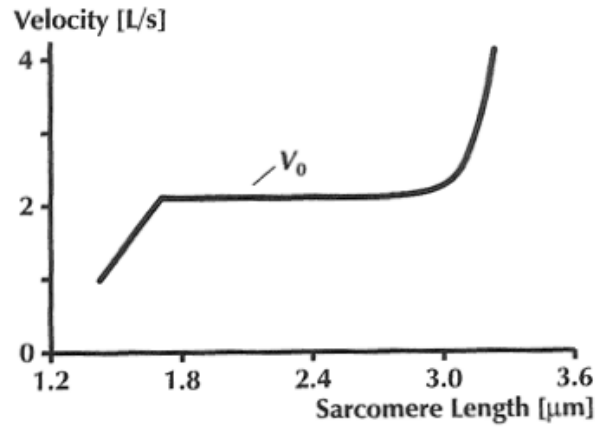


Figure 3.10: Maximal velocity of a shortening frog muscle over sarcomere length [EDMAN, 1979].

factor is necessary to keep the maximum contraction velocity, which is negative in equation 3.10, for decreasing activation  $q$  constant. The factors  $a$  and  $b$  in the equation of HILL [1938] were substituted by  $A_{rel} = a/F_0$  and  $B_{rel} = b/L_0$ . VAN SOEST [1992] also found that the maximum contraction velocity is not the same for the whole range of  $L$ . Therefore  $A_{rel} = A_{rel} * F(L)$  when  $L \geq L_0$  to keep the maximum contraction velocity constant in this area of the force-length relation. The dependency on the muscle fiber length can be seen in figure 3.12.

For  $L \geq L_0$  the maximum contraction velocity is:

$$v_0 = Factor(q) \frac{B_{rel}}{A_{rel}} L_0 \quad (3.11)$$

For  $L < L_0$ :

$$v_0 = Factor(q) F(L) \frac{B_{rel}}{A_{rel}} L_0 \quad (3.12)$$

For eccentric contractions the equation 3.10 does not fulfill the requirements. Therefore the equation is:

$$F = F_0 * q * \left( C_2 + \frac{C_1}{C_3 + v} \right) \quad (3.13)$$

The factors  $C_1$ ,  $C_2$  and  $C_3$  are calculated in the following way:

$$\begin{aligned} C_2 &= F(L) * F_{max/ecc} \\ C_4 &= C_2 - F(L) \\ C_3 &= C_4 \frac{Factor(q) B_{rel} L_0}{Slopefactor(F(L) + A_{rel})} \\ C_1 &= -C_4 C_3 \end{aligned} \quad (3.14)$$

According to GUENTHER [1997] the value for the *Slopefactor* is between 4 and 6. The value of

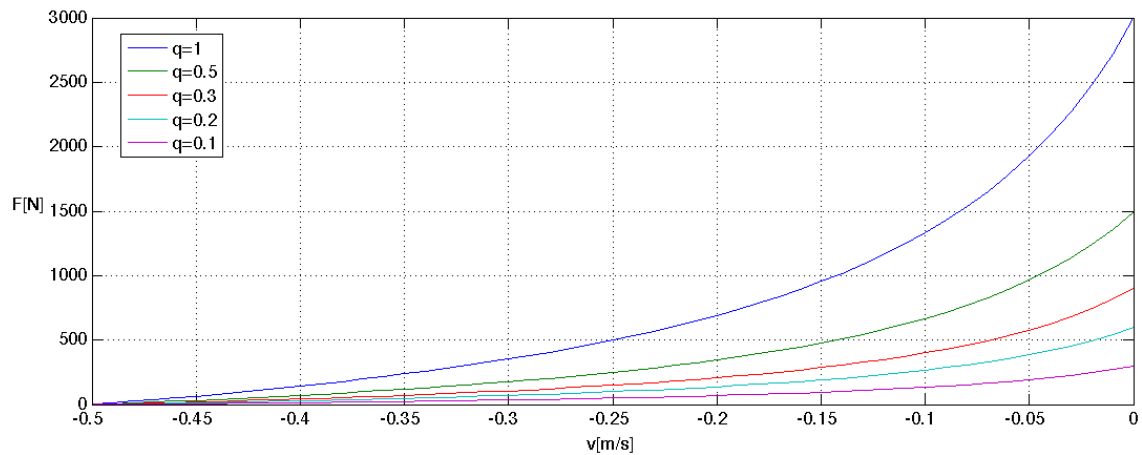


Figure 3.11: Force-velocity relation for concentric contractions with different activation levels  $q$ .  
 $F_0 = 3000N$ ,  $L_0 = 0.05m$ ,  $L/L_0 = 1$ ,  $v_0 = 0.5m/s$

$F_{max/ecc}$  is according to ZAJAC [1989] 1.8. All the other factors like  $Factor(q)$ ,  $A_{rel}$  and  $B_{rel}$  are the same as for concentric contraction.

### 3.3 Passive elements

So far only active force-length properties of skeletal muscle have been discussed. The term passive refers to the fact that this type of energy does not require metabolic energy. Two types of elastic elements will be discussed:

- Passive element in parallel with the contractile element
- Tendon element in series with the contractile element

Both elements were already mentioned by HILL [1938]. Figure 3.13 shows the arrangement of the elements in a Hill-type muscle model.

#### 3.3.1 Passive element in parallel with the contractile element

Pulling a muscle over a certain length results in a passive resistance. This kind of elastic resistance is associated with connective tissue structures surrounding the muscle fibers, fascicles and the entire muscle. The passive force is added to the active force of the contractile element (figure 3.14) [EPSTEIN and HERZOG, 1998].

$$F^m = F_{Active} + F_{Passive} \quad (3.15)$$

The active force-length curve depends on the activation level, the passive does not [ZAJAC, 1989]. According to [EPSTEIN and HERZOG, 1998, p. 52] the passive force length curve has to

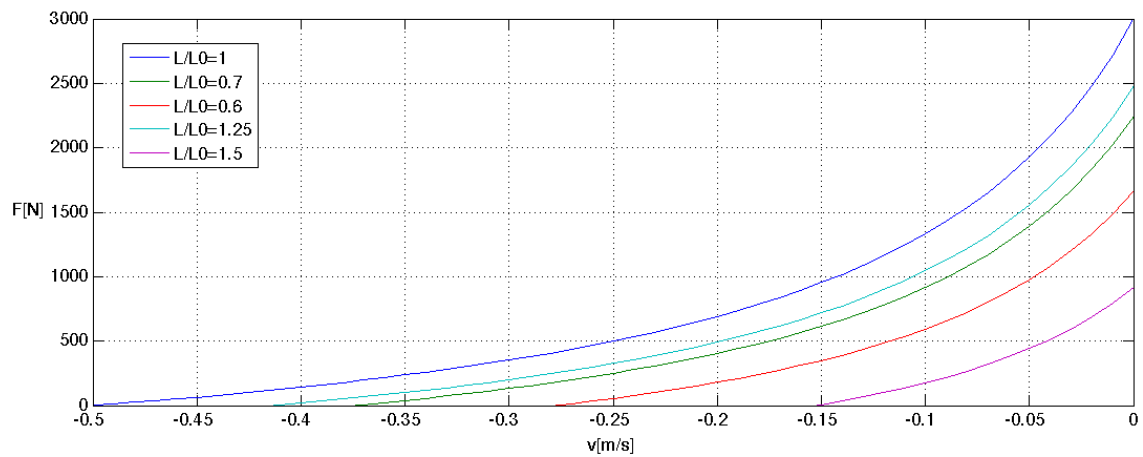


Figure 3.12: Force-velocity relation for concentric contractions with different muscle fiber lengths  $L/L_0$ .  $F_0 = 3000N$ ,  $L_0 = 0.05m$ ,  $q = 1$ ,  $v_0 = 0.5m/s$

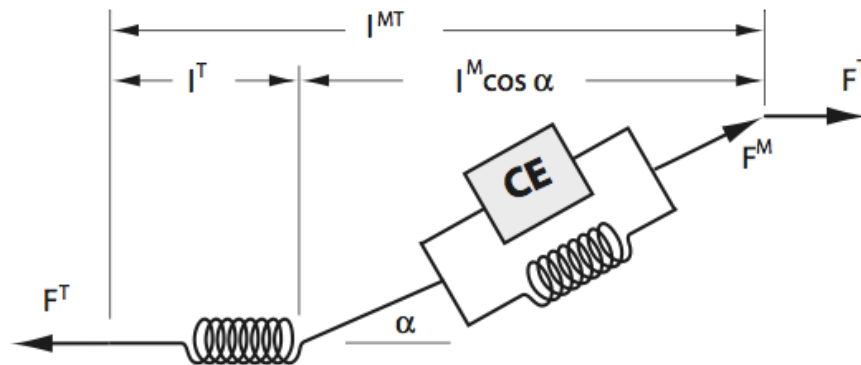


Figure 3.13: Hill type muscle model.  $F^M$  is the force generated by the contractile element.  $F^T$  is the force acting in the tendon.  $\alpha$  is the pennation angle of the muscle and  $l^{MT}$  is the length of the tendon  $l^T$  plus the length of the muscle  $l^M \cos \alpha$  [ARNOLD et al., 2010]

be determined for all different muscles separately because they look differently. In GUENTHER [1997]'s opinion the parameters of the passive element depend on the pennation angle, blood-flow in the muscle, temperature of the muscle and the fitness level. In some models i.e. ARNOLD et al. [2010], DELP [1990], ZAJAC [1989] and BUCHANAN et al. [2004] the force generation of the passive element starts at optimal muscle length (figure 3.14). Others, i.e. VAN SOEST [1992], mention a start for generating force at a normalized muscle fiber length of 1,4. GUENTHER [1997] uses a normalized muscle fiber length of 1,2. In my further examinations and simulations I will use the definition of ARNOLD et al. [2010] and DELP [1990] which can be seen in figure 3.14. The passive force starts at a normalized length of 1.0.

BUCHANAN et al. [2004] defines the normalized passive force-length  $f_{Passive}(l)$  relation as follows:

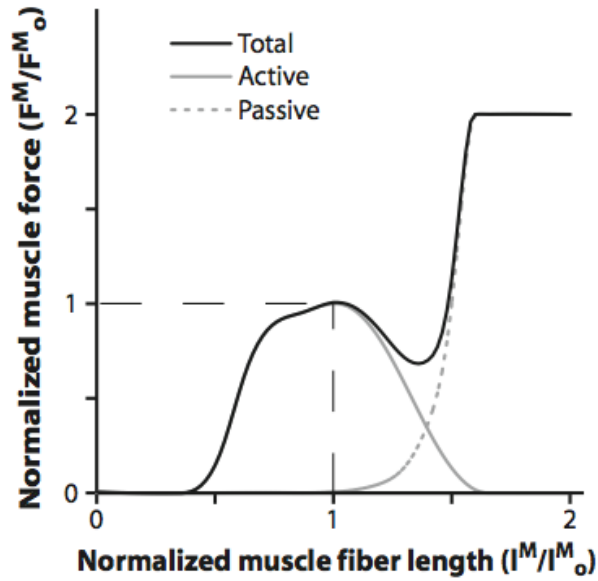


Figure 3.14: Active, passive and total force length curve used by ARNOLD et al. [2010] and DELP [1990]

$$f_{\text{Passive}}(l) = \frac{e^{10(\tilde{L}-1)}}{e^5} \quad (3.16)$$

$\tilde{L}$  is the normalized muscle fiber length  $L/L_0$ . Another form was shown by GUENTHER [1997]:

$$\begin{aligned} F_{\text{Passive}} &= K_{\text{Passive}}(L_{\text{Passive}} - L_{\text{Passive0}})^2 \\ L_{\text{Passive0}} &= L_{\text{Start}}L_0 \\ K_{\text{Passive}} &= \frac{F_{\text{PassiveMax}}F_0}{L_0(1 + \text{width} - L_{\text{Start}})^2} \end{aligned} \quad (3.17)$$

$K_{\text{Passive}}$  is the spring constant of the passive element.  $L_{\text{Start}}$  defines the normalized length where force generation starts. *width* defines the width of the force-length relation.  $F_{\text{PassiveMax}}$  defines the factor by which the maximum isometric force  $F_0$  is multiplied to generate maximum force in the passive element.  $L_0$  is the optimal fiber length and  $L_{\text{Passive}}$  is the current length of the parallel elastic element at time  $t$ . The equation of GUENTHER [1997] gives the model-designer the possibility to define individual tissue properties for each muscle.

### 3.3.2 Passive element in series with the contractile element

The elastic element in series with the contractile element represents the tendon which transmits the force from the muscle to the bone. It is also used to model the aponeurosis.

To describe the attributes of a tendon a stress-strain or force-elongation curve is used. This curves are like those of the passive elements in parallel with the contractile element - typically

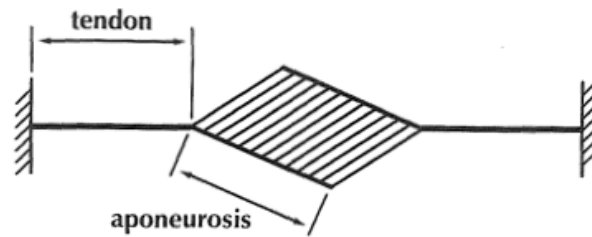


Figure 3.15: A unipennate muscle with an illustration of tendon and aponeurosis [EPSTEIN and HERZOG, 1998]

nonlinear. Tendon stress  $\sigma^T$  is defined as the ratio of the tendon force  $F^T$  to tendon cross sectional area  $A^T$ . According to RIGBY et al. [1959] tendons have a toe region for strains from 1-3% (figure 3.16) followed by a stiffer region reaching a tangent elastic modulus of 1.0 - 1.5GPa. ZAJAC [1989] observed that the strain in the tendon is 3.3% when the muscle generates maximum isometric force  $F_0$ . The failure strain is at approximately 8-10% - force reaches  $3.5F_0$  or a stress of 100MPa. Tendons also show a slight viscoelasticity. During cyclic loading and unloading the energy released by tendons is about 85-95% of the energy which was received (figure 3.16). A high amount of the energy is used as mechanical work when the muscle-tendon complex is unloaded [EPSTEIN and HERZOG, 1998]. The properties mentioned differ for any muscle and so they have to be determined for each muscle when doing a very accurate model.

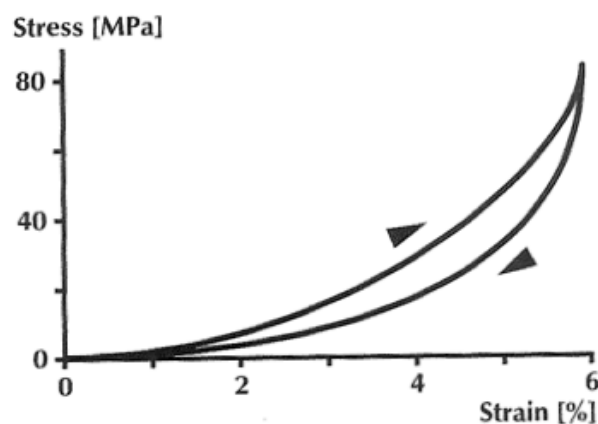


Figure 3.16: Stress-strain curve of a tendon. For lower strains the tendon shows a lower stiffness (toe region). Increasing the strain leads to a higher stiffness (linear region) [EPSTEIN and HERZOG, 1998]

Under the microscope tendon and aponeurosis have a wave-like crimp structure in the unstretched state. This wavy structure disappears with initial elongation in the toe region. As a result tendons and aponeurosis can elongate but do not transmit any force to the bone [EPSTEIN and HERZOG, 1998]. The length at which tendons start to generate force is the tendon slack length

$l_s^t$ . The strain in the tendon is computed with the following formula:

$$\epsilon^t = \frac{l^t - l_s^t}{l_s^t} \quad (3.18)$$

In my models I use the formulation of ZAJAC [1989] to describe the normalized tendon's force  $\tilde{F}^t$  as follows:

$$\begin{aligned} \tilde{F}^t &= 0 & \epsilon^t &\leq 0 \\ \tilde{F}^t &= 1480.3\epsilon^t{}^2 & 0 < \epsilon^t < 0.0127 \\ \tilde{F}^t &= 37.5\epsilon^t - 0.2375 & \epsilon^t &\geq 0.0127 \end{aligned} \quad (3.19)$$

To compute the actual tendon force  $F^t$  the normalized tendon force has to be multiplied with the maximum isometric force [ZAJAC, 1989]:

$$F^t = \tilde{F}^t F_0 \quad (3.20)$$

### 3.3.3 Angle of pennation

In most muscles the fiber line of action is not the same as the muscle line of action. The angle between these both can be described with the pennation angle (see figure 3.17). According to figure 3.5 multipennate muscles have more than one angle of pennation.

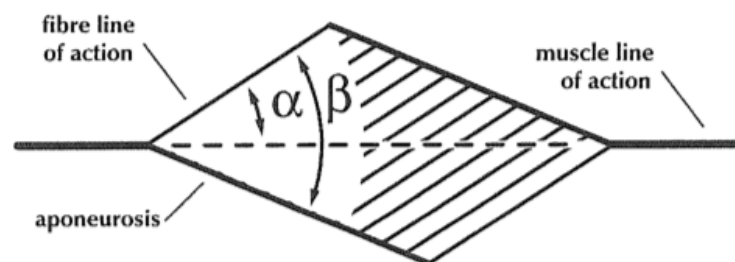


Figure 3.17: The angle of pennation  $\alpha$  defined as the angle between the line of action of the fiber and the line of action of the muscle.  $\beta$  represents the angle between the aponeurosis and the fiber line of action [EPSTEIN and HERZOG, 1998]

WICKIEWICZ et al. [1983] measured the angle of pennation for 27 human lower limb muscles in three cadavers. He defined only one angle of pennation for each muscle. The maximum pennation rarely exceeds 25-30°. To compute the force in the muscle line of action (which is the tendon force) the force produced in the contractile element is multiplied with the  $\cos(\alpha)$ :

$$F^t = F^m \cos(\alpha) \quad (3.21)$$

WAGEMANS and VAN LEEMPUTTE [1989] showed that the angle of pennation changes with the force output and the fiber length. The pennation angle increases with increasing force production

at a given muscle length and also increases with shortening muscle at a given force. KAWAKAMI et al. [1998] showed with ultrasound that the medial gastrocnemius changes the pennation angle from  $22^\circ$  to  $67^\circ$  depending on the joint angle and muscle activation. However many models calculate only with one pennation angle (ARNOLD et al. [2010], DELP [1990]) because measuring the pennation angle over all muscle lengths and forces makes a lot of work and the effect on the actual tendon force is not that big for angles below  $20^\circ$  [BUCHANAN et al., 2004]. For large angles like in the triceps surae the pennation angle can have a significant effect. In my models I use the formulation (equation 3.22) of SCOTT and WINTER [1991] to calculate the pennation angle  $\alpha(t)$  in a contracting muscle. SCOTT and WINTER [1991] assume that the muscles have constant thickness and volume.

$$\alpha(t) = \sin^{-1} \left( \frac{L_0 * \sin(\alpha_0)}{L(t)} \right) \quad (3.22)$$

$L(t)$  is the current fiber length at time  $t$ ,  $\alpha_0$  is the pennation angle at optimal fiber length  $L_0$ .

### 3.4 Activation dynamics

Muscles are excited electrically over nerve axons. These axons have their origin in the central neural system and the endings in the muscle fibers. One functional and smallest unit to generate force is called motor unit. It consists of one axon and the muscle fibers excited by this axon. As a result one muscle can be represented by  $n$  motor units being controlled by  $n$  nerve axons.

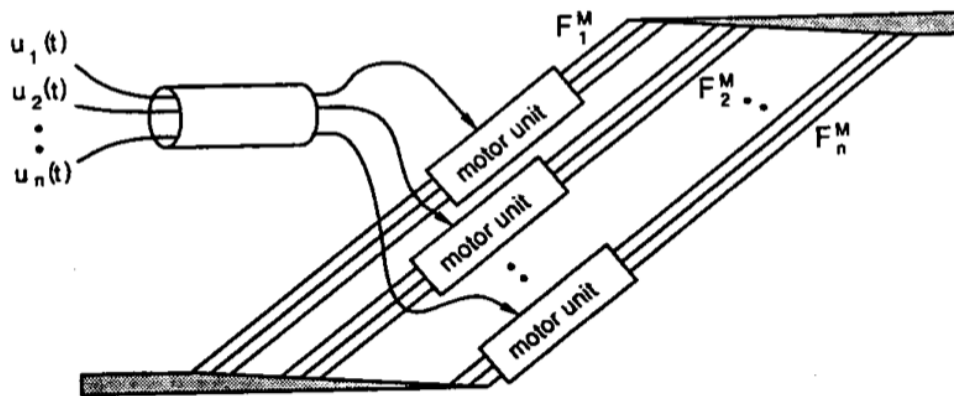


Figure 3.18: Schema of the collective function of motor units of one muscle. Each motor unit is functionally disjoint from the others, including the set of muscle fibers innervated by each nerve axon. The action-potential discharge pattern ( $u_i(t)$ ) of each axon  $i$  excites the muscle fibers of that motor unit  $i$  and generates the collective force  $F_i^M$ . [ZAJAC, 1989, p. 4]

To get from the electric excitation to the contraction of the muscle and a power output many physiological, histochemical and biochemical processes have to be executed. All these processes

need time and as a result the muscle needs a certain time to produce it's maximum force. It takes a certain time to increase on one hand and a certain time on the other hand to decrease the force. In the literature three different models are described:

- ZAJAC [1989]
- HATZE [1977]
- SUST [1987], SUST et al. [1991]

SUST [1987] describes only the activation-pattern and no deactivation. Therefore I won't discuss this theory further.

### Hatze's activation dynamics

This model tries to simulate the electro-chemical microscopic actions within a muscle fiber. It describes the changing concentration of free  $Ca^{++}$ -ions  $\gamma$  during a stimulation.  $\gamma$  is normalized to its maximum value  $c = 1.473 * 10^{-6} Mol$ . When a muscle is completely deactivated the concentration  $\gamma = \gamma_0 = 10^{-3}$ . As a result the free concentration  $\gamma$  is  $\gamma_0 \leq \gamma \leq 1$ . The free concentration  $\gamma$  can be described with the differential equation 3.23.

$$\dot{\gamma} = M_h(STIM - \gamma) \quad (3.23)$$

$M_h$  is the time constant for activation and deactivation. In Hatze's case they are the same, which is not the result of measurements stated in the literature [GUENTHER, 1997]. In reality the deactivation takes longer than the activation.  $STIM$  is between 0 and 1 and describes the neural stimulation of the muscle fiber. To get from the free  $Ca^{++}$  concentration to the bound  $Ca^{++}$  concentration HATZE [1977] uses equation 3.24.

$$q(L, \gamma) = \frac{q_0 + [\rho(L)\gamma]^2}{1 + [\rho(L)\gamma]^2} \quad (3.24)$$

$\rho(L)$  is used to describe the overlapping of the actin and myosin in the sarcomere:

$$\rho(L) = \frac{1.373 * 6.62 * (2.9 - 1)}{2.9 * \left(\frac{L_0}{L}\right) - 1} \quad (3.25)$$

### Zajac's activation dynamics

In comparison to HATZE [1977], ZAJAC [1989] describes the activation dynamics in a more macroscopic way. He links the neural excitation and the contractile machinery via a variable called muscle activation (see figure 3.19). The muscle activation  $a(t)$  refers to the  $Ca^{++}$  concentration, which has important characteristics: the rate constant for activation is higher than for deactivation and the activation has a saturation.

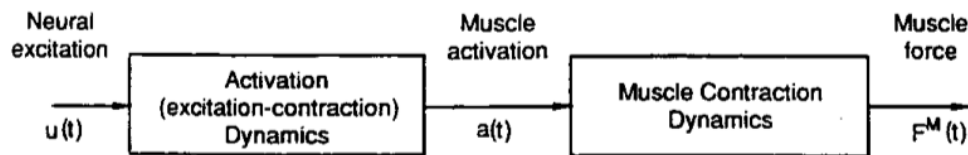


Figure 3.19: Muscle tissue dynamics. Neural excitation  $u(t)$  acts through activation dynamics to generate an internal muscle tissue state  $a(t)$  (muscle activation), which is associated with the  $Ca^{++}$  activation of the contractile process. Via muscle contraction dynamics, this activation energizes the cross-bridges and muscle force  $F^M(t)$  is developed. [ZAJAC, 1989, p. 5]

The only neuronal measurable parameter is the EMG (=neural excitation  $u(t)$ ) and so ZAJAC [1989] describes the muscle force with only one input signal - the EMG. The processed and normalized EMG-signal is used as the  $STIM$  parameter in the interval  $0 \leq STIM \leq 1$ . The muscular activity  $a$  (means active state and is equal to  $q$  in the formulation of HATZE [1977]) is defined as the relative isometric force at optimal muscle length  $L_0$ . To describe the activation ZAJAC [1989] defined the following differential equation 3.26.

$$\dot{a} + \left[ \frac{1}{T_{act}} (\beta + [1 - \beta] STIM) \right] a = \left( \frac{1}{T_{act}} \right) STIM \quad (3.26)$$

$T_{act}$  is the time constant to activate the muscle fully when  $STIM = 1$ .  $\beta$  is the ratio of  $T_{act}/T_{deact}$  with  $T_{deact}$  defining the time constant to reach full deactivation with  $STIM = 0$ .

### Comparison of the activation dynamics

Figure 3.20 shows that the activation of the muscle is nearly the same for both models. The deactivation routine in comparison is different. In the case of Hatze the process to reduce or pump off the ions is a non exponential one - at the beginning it takes longer to reduce the concentration.

HATZE [1977] describes a model which has the focus on the microscopic actions in a fiber - in detail it describes the changing  $Ca^{++}$  concentration during stimulation. Looking at equation 3.23 will show that the model will always assume that **all** fibers are recruited which is not the truth (GUENTHER [1997]). The model might have more importance in the future when measurements will be available for determining microscopic electro-chemical reactions during an in vivo experiment.

In the activationdynamics of ZAJAC [1989] there is no dependency on internal unknown parameters. For proving the model of ZAJAC [1989] only the EMG and the isometric force have to be observed. Additionally the time constants for activation and deactivation are independent from each other. In my case I'm using Zajac's model because the aim of the model will be to perform a forward dynamic simulation with an EMG-signal as an input.

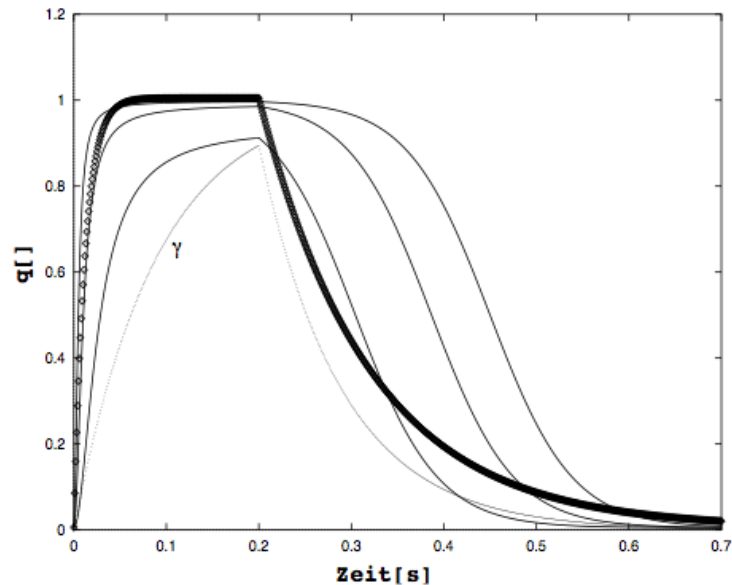


Figure 3.20: Comparison of Zajac's and Hatze's activation function. At time  $t = 0s$  :  $q = q_0$  and  $STIM = 1$  until  $t = 0.2s$ , then  $STIM = 0$ . Fat line: Zajac; thin line: Hatze with  $L/L_0 = 1.5, 1, 0.5$  top-down. Hatze's free concentration  $\gamma$  is also shown [GUENTHER, 1997].

## 3.5 Model parameters

### 3.5.1 Muscle parameters

In this chapter I list all muscle modeling parameters I used. This includes the individual muscle parameters in table 3.2 and the global muscle parameters in table 3.1. The individual parameters are adopted from ARNOLD et al. [2010] and global ones from GUENTHER [1997] and ARNOLD et al. [2010]. These parameters are mostly used in the literature and the model from ARNOLD et al. [2010] is implemented in OpenSim which makes it very comfortable to compare and validate my results.

$width$ []	$a$ []	$b$ []	$v_0$ [m/s]	$T_{act}$ [s]	$\beta$ []	$F_{0ecc}$ [N]	$L_{start}$ []	$F_{PEEmax}$ [N]
0.6	0.25	0.25	$10 * L_0/s$	0.01	0.25	$1.8F_0$	$L/L_0$	$2F_0$

Table 3.1: Global muscle parameters

$width$  defines the range of force in the normalized force-length relation.  $a$  and  $b$  are constants from Hill's equation.  $v_0$  defines the maximum contraction velocity.  $T_{act}$  and  $\beta$  define the activation- and deactivation-time constant in Zajac's equation.  $F_{0ecc}$  gives the maximum force during eccentric contraction.  $L_{start}$  and  $F_{PEEmax}$  are parameters to define the parallel elastic elements: The normalized fiber length where force production starts and maximum force in the parallel elastic element.

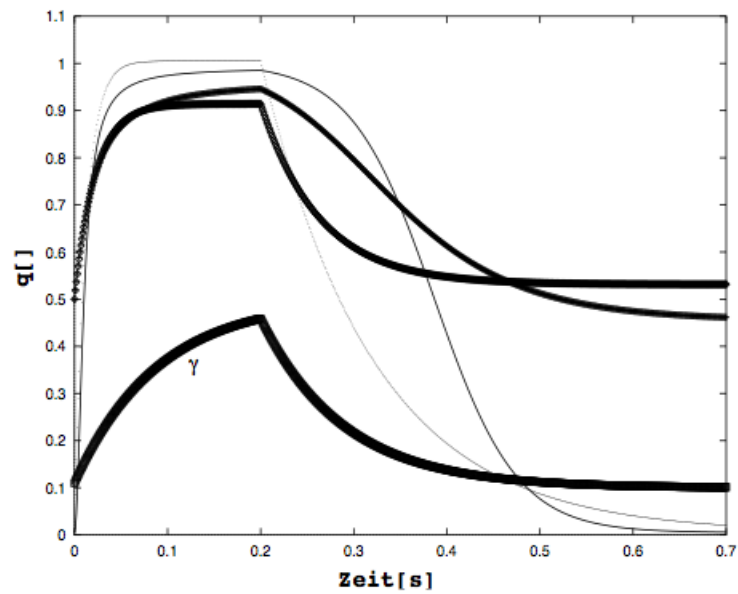


Figure 3.21: Comparison of different activation dynamics. Thin lines: Zajac and Hatze ( $L/L_0 = 1$ ) from figure 3.20. Upper fat lines: Zajac and Hatze in comparison.  $t = 0s : q = 0.5$  and  $STIM = 0.5$  until  $t = 0.2s$ , then  $STIM = 0.1$ . Hatze's free concentration  $\gamma$  is also shown in the lower fat line [GUENTHER, 1997].

Muscle	PCSA[ $cm^2$ ]	Peak force $F_0[N]$	Optimal fiber length $L_0[cm]$	Tendon slack length $l_s^t[cm]$	Pennation angle $\alpha[^\circ]$
Soleus	58.2	3549	5.0	25	25
Gastrocnemius medial head	25.5	1558	6.0	39	17
Gastrocnemius lateral head	11.2	683	6.4	38	8
Tibialis anterior	11.0	905	9.8	22.3	5

Table 3.2: Individual muscle parameters: Peak force was calculated by multiplying the PCSA with  $61N/cm^2$ . Pennation angle gives the pennation  $\alpha$  at optimal fiber length  $L_0$ .

### 3.5.2 Skeletal parameters

In my models I simulate two dimensional motions around the ankle joint. The ankle joint which is described in chapter 2 is a very complex structure. It contains three individual joints. In the literature (ARNOLD et al. [2010], DELP [1990]) the three joints are usually combined to simplify the model. During my simulations I also use a simplified „one joint“-ankle. For calculating the moment of inertia of the foot in the ankle joint I adopted the values from ARNOLD et al. [2010] - listed in table 3.3.

Bone	Moment of inertia I [ $kgm^2$ ]	Mass [kg]	Radius of center of mass [cm]
Talus	0.001	0.1	0
Calcaneus and Metatarsus	0.0041	1.25	5.2
Toes	0.0001	0.2166	16.9

Table 3.3: Sekeletal parameters

The resulting moment of inertia around the z axis (figure 3.22) can be calculated with the parallel axis theorem:

$$I_{zz} = I_{Talus} + I_{Calcaneus} + m_{Calcaneus}r_{Calcaneus}^2 + I_{Toes} + m_{Toes}r_{Toes}^2 = 0.01476kgm^2 \quad (3.27)$$

### 3.5.3 Movement definitions

The possible ankle motions relevant for my simulations are shown in figure 3.22. A plantarflexion is defined as a negative value in my model. A dorsiflexion is defined as a positive ankle angle.

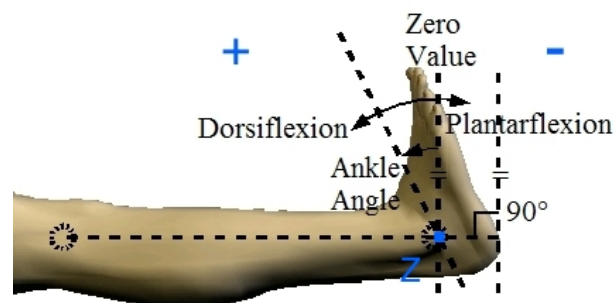


Figure 3.22: Definition of the ankle movements.

## 4 Electromechanical analogies

Between the two fields of mechanics and electrical engineering exists an analogy. This means that a physical quantity from mechanics can be transformed to a physical quantity in electronics. The relations between the quantities in one system are the same as the relationships in the other system. Due to this fact a mechanical system built up with elementary parts (springs, dampers and masses) can be replaced by an electrical circuit with analogue electrical parts (resistors, condensators and inductivities). The big advantage is the well implemented electric circuit analysis which makes it much easier to analyze mechanical systems when they are transformed to electrical circuits. Between mechanics and electronics two analogies are available [ZELLER, 2009, p. 12-14]:

- Force-current analogy
- Force-voltage analogy

Using the second analogy (force-voltage) constructs no equivalent topology of the network and therefore this analogy is not used in my simulations. Table 4.1 shows the analog quantities for the elementary mechanical quantities mass, damping, spring and compliance.

Mechanics		Electronics	
Force	$F(t)$	$i(t)$	Current
Velocity	$v(t)$	$u(t)$	Voltage
Damper	$d = F/v$	$1/R = i/u$	Conductance
Mass	$m = \frac{F}{dv/dt}$	$C = \frac{i}{du/dt}$	Capacitance
Spring	$k = \frac{dF/dt}{v}$	$\frac{1}{L} = \frac{di/dt}{u}$	Inductance

Table 4.1: Linear motion electromechanical analogies for a force-current analogy

Performing a rotational movement like in a human joint, table 4.2 shows the analogies. In my simulations I use only these analogies because of the rotational movements performed in our joints.

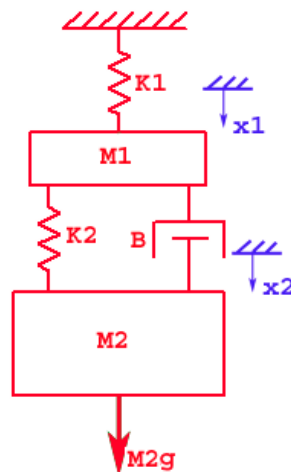
Mechanical topologies are represented as equivalent electrical circuits in form of a dipole. The relation between the input signal and the output signal is described with differential equations.

Mechanics		Electronics	
Moment	$M(t)$	$i(t)$	Current
Angular velocity	$\omega(t)$	$u(t)$	Voltage
Damper	$d = M/\omega$	$1/R = i/u$	Conductance
Moment of inertia	$I = \frac{M}{d\omega/dt}$	$C = \frac{i}{du/dt}$	Capacitance
Spring	$k = \frac{dM/dt}{\omega}$	$\frac{1}{L} = \frac{di/dt}{u}$	Inductance

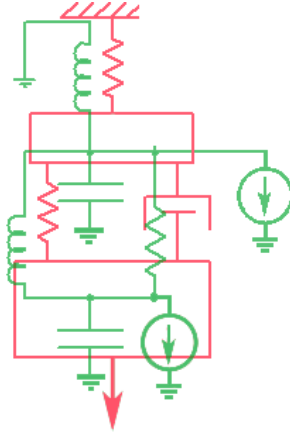
Table 4.2: Rotational electromechanical analogies for a force-current analogy

## 4.1 Example for converting a mechanical system into an electrical circuit

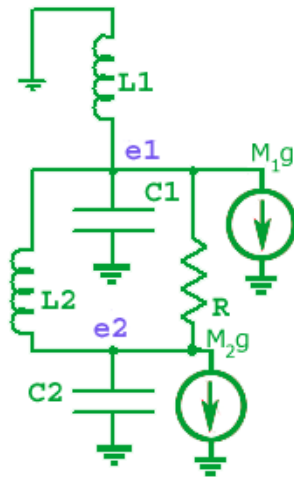
The following simple mechanical system will be transformed into an electrical circuit [SWARTH-MORE]:



All mechanical elements are replaced by their electric analogs. Springs convert to inductors, masses to capacitors. To avoid relative motions of the masses the capacitors are grounded. The masses act as force generators which are simulated by current sources in the electric circuit.



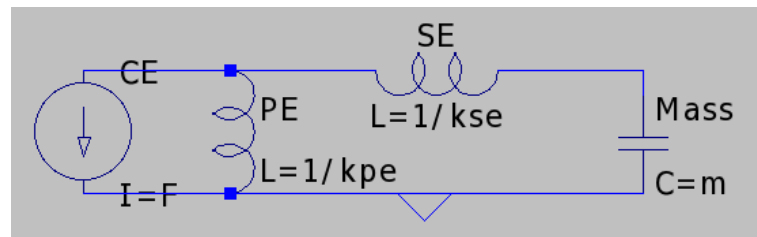
Each position in the mechanical system becomes a node in the electrical equivalent ( $x_1 \rightarrow e_1$ ,  $x_2 \rightarrow e_2$ ). The following circuit can be used to simulate the mechanical system.



The voltages at the nodes  $e_1$  and  $e_2$  represent the velocities of the masses  $M_1$  and  $M_2$ .

## 4.2 Hill's electrical equivalent

Hill's model (see figure 3.13) can be replaced by an electrical circuit as well and is the basis for my simulations. The following circuit shows a muscle acting on a mass. The contractile force generating element is replaced by a current source. The parallel elastic and serial elastic elements are replaced by inductors. According to table 4.1 the values of the inductors are the inverse of the spring-constants. In this simple case the inductors have a linear characteristic which is not the case as discussed in chapter 3.3. The mass which is moved by the muscle in form of a linear motion is replaced by a capacitor. The value of the capacitance is the mass in kg.



As already mentioned in a human joint many muscles have to be considered and they induce a rotational movement of body segments. Therefore the capacitance represents the inertial moment of the masses involved in the joint. The current of the current source then represents the moment generated by the muscle. Measuring the voltage at the capacitance gives the angular velocity of the joint movement. To compute the actual angle of the joint the voltage has to be integrated over time.

## 5 Model control

During my work I carried out two ways of controlling the muscle model. Both will be explained in this section and the results can be seen in chapter 6. One approach calculates the joint-moment with the combination of muscle and tendon (musculo-tendon-unit). The basic input is the musculo-tendon-length. In the second approach the moment is calculated only with the fiber length as the basic input and the tendon is not considered. The two ways are both used in the literature. The tendon-approach by ARNOLD et al. [2010], DELP [1990], ZAJAC [1989], BUCHANAN et al. [2004]. GUENTHER [1997] and PROCHEL [2009] use the second control-architecture.

### 5.1 Musculo-Tendon-control

The tendon-force induces a joint moment, but as explained in the chapters before the force depends on many factors. It depends especially on the motor which is the contractile element. It can be said that the actuator acting on the joint is a unit of muscle and tendon - musculo-tendon unit MTU. Therefore the force is called musculo-tendon-force  $F^{mt}$  and can be written as shown in the following equation [BUCHANAN et al., 2004]:

$$F^{mt} = (\alpha, t) = f(a, l^{mt}, v^{mt}, F_0, L_0, l_s^t, \alpha_0) \quad (5.1)$$

The musculo-tendon-force depends on individual musculo-skeletal parameters which are assumed not to change over time: maximal isometric muscle force  $F_0$  at optimal fiber length  $L_0$ , tendon slack length  $l_s^t$  and the pennation angle  $\alpha_0$  at optimal fiber length  $L_0$ . Furthermore the musculo-tendon-force depends on the activation level  $a$ , current musculo-tendon-length  $l^{mt}$  and velocity  $v^{mt}$ . The function depends on the force-length and on the force-velocity relation of the contractile element. Rewriting equation 5.1 shows how the muscle-tendon force is actually calculated:

$$\begin{aligned} F^{mt}(\alpha, t) &= F^t \\ &= [F_{Active} + F_{Passive}] \cos(\alpha) \\ &= [f_{Active}(l) f(v) a(t) F_0 + f_{Passive}(l) F_0] \cos(\alpha) \end{aligned} \quad (5.2)$$

The tendon-force is the muscle-force, which adds up the forces of the active contractile element  $F_{Active}$  and passive elastic element  $F_{Passive}$  (calculated with equation 3.15), multiplied with the triangulated form of the pennation angle (3.21). The active and passive forces can be rewritten in the form of normalized force-length relations (equations 3.3, 3.4, 3.16 and 3.17)  $f_{Active}(l)$  and

$f_{Passive}(l)$ . Both are multiplied with the maximum isometric force  $F_0$ , the active force additionally with the normalized force-velocity  $f(v)$  and the activation  $a(t)$ .

As shown in figure 5.1 in my model I measure the joint-angle by integrating the rotational velocity (voltage in electrical simulation) over time. Furthermore I use the musculo-tendon-length  $L^{MT}$  over the joint-angle relation and the tendon-slack length  $L_s^T$  from ARNOLD et al. [2010] as an input to compute the fiber length  $L^M$ :

$$L^M = L^{MT} - L_s^T - \frac{F^T}{k^T} \quad (5.3)$$

$k^T$  is the tendon stiffness which can be calculated from equation 3.19. Knowing the fiber length, the normalized active and passive force of the contractile element can be calculated (equation 3.16 and equation 3.4). By subtracting the passive force from the current tendon force, the active force in the contractile element can be computed:

$$f_{Active} = \frac{F^T}{F_0 \cos(\alpha)} - f_{Passive} \quad (5.4)$$

The pennation angle is calculated with equation 3.21. Now the value of the normalized force velocity relation can be calculated:

$$f(v) = \frac{f_{Active}}{a(t)f(l)} \quad (5.5)$$

The activation  $a(t)$  is computed with the differential equation 3.26 of ZAJAC [1989] with a stimulation level as an input. Problems occur when  $a(t)$  or  $f(l)$  become zero because the equation is not solvable anymore. To overcome this  $f(v)$  is set to 1.8 (maximum eccentric force) when  $f(v) \geq 1.8$  or 0.01 when  $a(t) = 0$  or  $f(l) = 0$ . This guarantees that the muscle acts with maximum force when getting stretched. In the next step the velocity of the contractile element will be computed by taking the inverse of the force velocity curve (equation 3.8):

$$v_M = -v_0(-3e^{f(v)-0.02} - 0.1e^{12f(v)-1.5} - 0.052618) \quad (5.6)$$

The force in the tendon is computed with a first order differential equation from ZAJAC [1989]:

$$\dot{F}^T = k^T(v_{MT} - v_M) \quad (5.7)$$

The musculo-tendon velocity  $v_{MT}$  is a result of differentiating the musculo-tendon-length  $L^{MT}$ . The final step is to calculate the joint moment(electrical current in my model) by multiplying the tendon force with the moment arm . The moment arm over the joint-angle data is also adopted from ARNOLD et al. [2010].

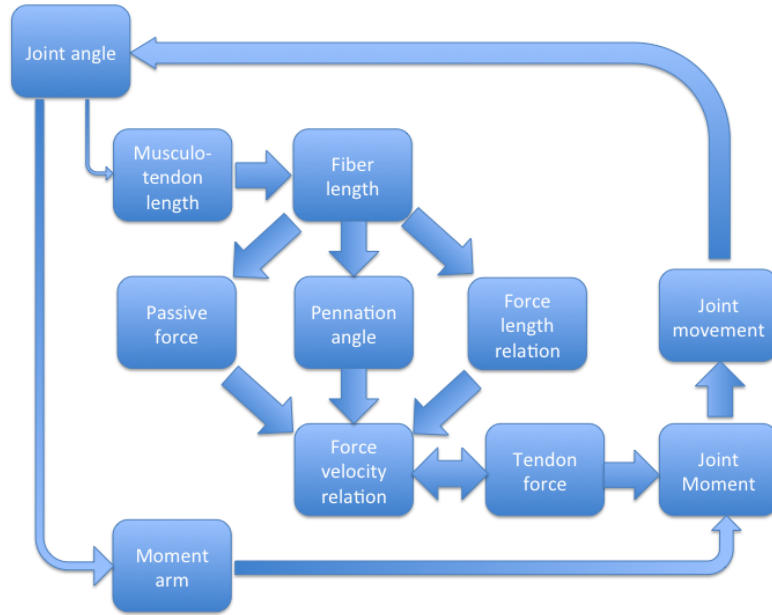


Figure 5.1: Block-diagram of the tendon-controlled model

## 5.2 Muscle-fiber-length-control

The second approach I used to control my model is the use of the muscle-fiber-length as the primary input. The block-diagram in figure 5.2 shows an overview of my control system. From the joint movement the current joint angle can be calculated by integrating the circular speed of the joint (measuring voltage). ARNOLD et al. [2010]'s relation between the joint angle and fiber length is used to determine the fiber length. Having the fiber length, the individual muscle parameters  $F_0$ ,  $L_0$  and the global parameters from table 3.1 is enough to compute the passive force (equation 5.8) and the normalized force in the active force length relation (equation 5.9).

$$f_{Passive}(l) = \frac{e^{10(\bar{L}-1)}}{e^5} \quad (5.8)$$

$$f_{Active}(l) = -\frac{1}{width^2} * \left(\frac{L}{L_0}\right)^2 + \frac{2}{width^2} \left(\frac{L}{L_0}\right) - \frac{1}{width^2} + 1 \quad (5.9)$$

Differentiating the fiber length over time results in a contraction velocity. Combining the active fiber parameters, the contraction velocity and normalized force from the force length relation with equation 5.10 leads to the muscle force.

$$F = \frac{-q * F_0 * (A_{rel} * v + B_{rel} * F(L) * Factor(q) * L_0)}{v - B_{rel} * Factor(q) * L_0} \quad (5.10)$$

Beside the mentioned factors, the activation which is computed with Zajac's equation 3.26 is also an input factor. The tendon force is computed by adding the passive force to the active force and multiplying it with the  $\cos(\alpha)$ . The pennation angle is calculated with equation 3.22. In order to compute the joint moment (current), the moment arm which depends on the joint angle is needed. The relation between moment arm and joint angle is also adopted from [ARNOLD et al., 2010]. Within this control mechanism the properties of the tendon are in comparison to the first control approach completely neglected.

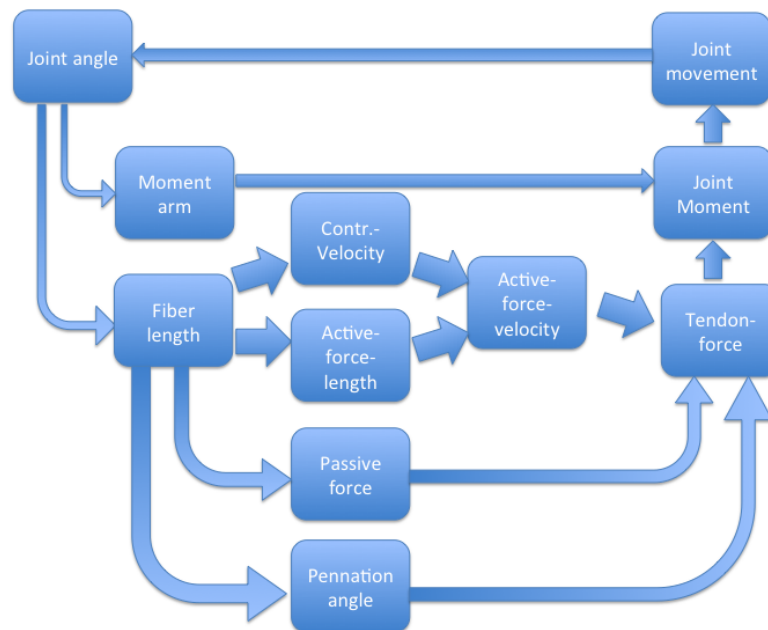


Figure 5.2: Block-diagram of the fiber-length-controlled model

### 5.3 Differences between electrical simulation and numerical simulations

During numerical simulations (ARNOLD et al. [2010], DELP [1990], GUENTHER [1997], BUCHANAN et al. [2004], THELEN [2003], THELEN et al. [2003]), which are normally performed when calculating a forward dynamic problem, the model control is different to my control with an electrical simulation.

The activation is calculated the same way as I do in my models - in most cases as suggested by ZAJAC [1989]. At simulation start the tendon length is computed with a given musculo-tendon-length, tendon slack length and initial tendon force. Knowing the tendon length leads to a strain in the tendon. This is used to obtain the tendon force which is applied on the body segment. By knowing the muscle-tendon-length and the tendon length (figure 3.13) the muscle length can be computed. With this information the active- and passive-force length value is calculated. The

next step calculates the normalized force-velocity value. Building the inverse of the normalized force-velocity value leads to the contraction velocity of the muscle. In the final step the muscle length for the next iteration is calculated by integrating the velocity. With the new muscle length and the known musculo-tendon-length the tendon length can be computed again. The loop starts again by calculating the new strain and the new tendon force applied on the segment.

During my electrical simulations with my first control-mechanism I measure the voltage (circular speed) on my capacitance (moment of inertia) and integrate it over time to compute the joint angle. With this information the musculo-tendon-length is calculated. Building the derivative leads to the musculo-tendon-velocity. The velocity of the muscle is also calculated by building the inverse of the force-velocity value. The tendon force is then calculated with the first order differential equation:

$$\dot{F}^T = k^T(v_{MT} - v_M) \quad (5.11)$$

Using the second control-approach does not include any calculation of the tendon length. It only uses the muscle fiber contraction velocity (derivative of the fiber length) to compute the force in the contractile element. The tendon force is then calculated by multiplying the accumulated passive and active force with the pennation angle.

$$F^T = (F_{Active} + F_{Passive})\cos(\alpha) \quad (5.12)$$

In my model I use programmable voltage or current sources in LTspice IV to perform mathematical tasks like building a derivative. The values of the sources can be compared with variables in a programming language.

## 6 Results

During my work I carried out different simulation cases. The first case is simulated with both control mechanisms described in chapter 5. The simulations are always done for the human ankle joint (figure 3.22) involving different muscles with different stimulation-patterns. The different simulation cases are:

1. M. soleus acts on the ankle joint without gravity
2. M. soleus, M. med. gastrocnemius, M. lat. gastrocnemius and M. tibialis ant. act on the ankle joint without gravity

All simulations were done with the software LTspice IV (1630 McCarthy Blvd., Milpitas, CA) in Windows Vista. Furthermore all simulations were carried out with OpenSim (3DGaitModel 2392) for comparison with the results of the electrical simulation. The gravity was not included to reduce the potential differences between the two types of simulations.

### 6.1 Simulation case 1

A single muscle (M. soleus) is innervated to perform a plantarflexion in the ankle joint. The gravity is set to zero. The stimulation signal representing the EMG is shown in figure 6.1. The same diagram shows the activation calculated with Zajac's differential equation 3.26.

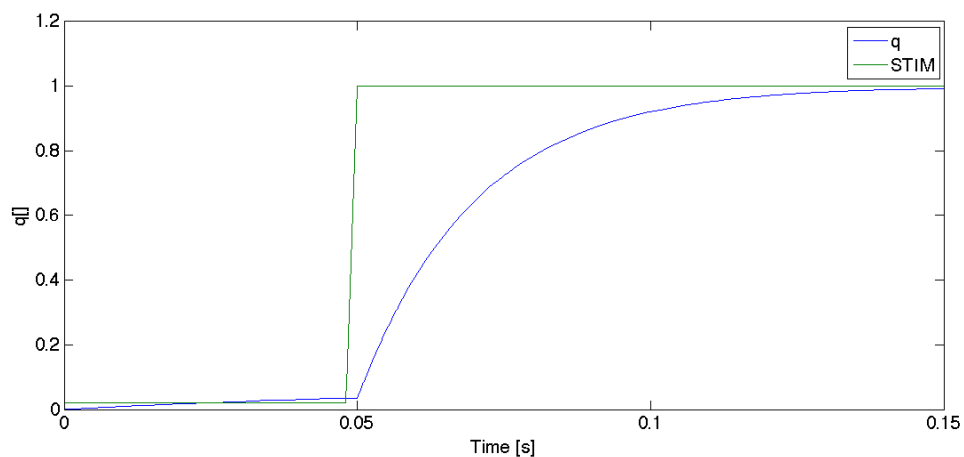


Figure 6.1: Green: Stimulation signal. Blue: Muscle activation  $q$ .

Pennation angle, tendon length and fiber length for both control mechanisms are shown in figures 6.2, 6.3 and 6.4.

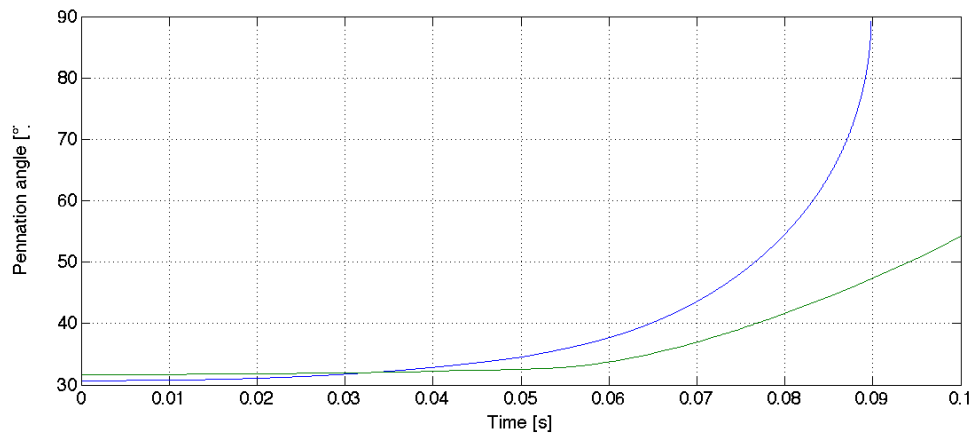


Figure 6.2: Pennation angle between contractile element and tendon. Green: Fiber-length-controlled. Blue: Musculo-tendon-controlled.

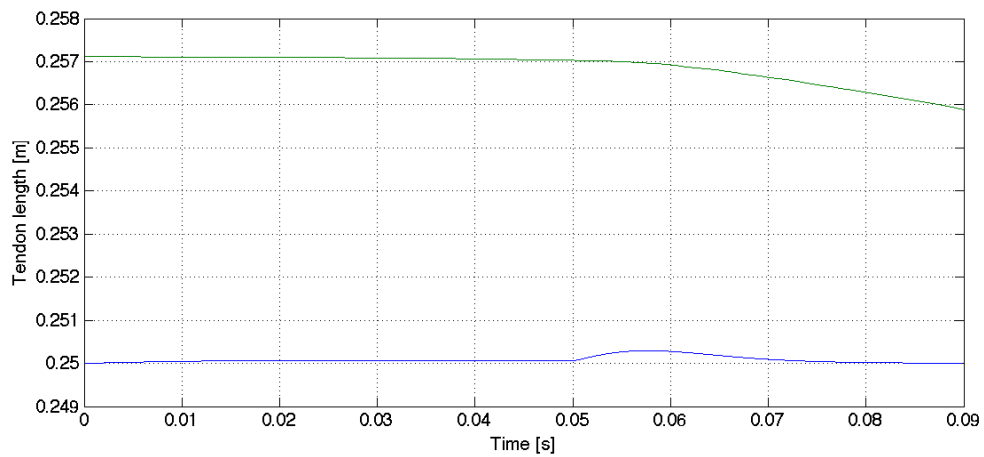


Figure 6.3: Length of the tendon during contraction. Green: Fiber-length-controlled. Blue: Musculo-tendon-controlled.

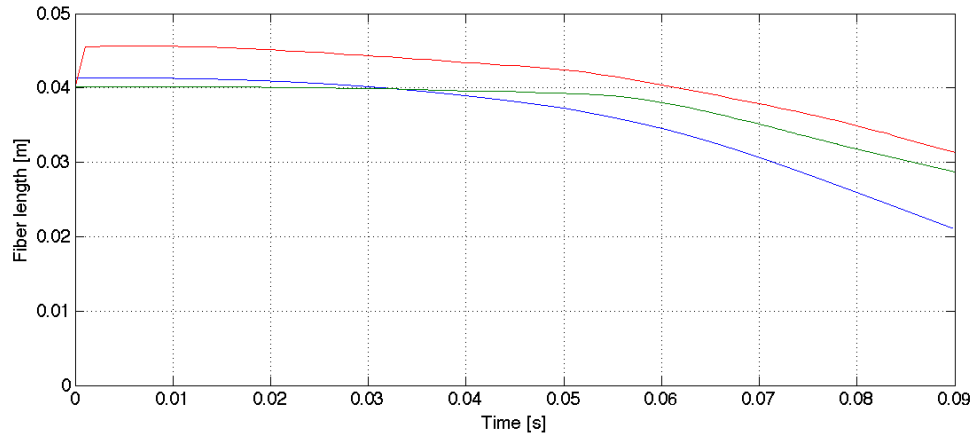


Figure 6.4: Length of the contractile element over time. Green: Fiber-length-controlled. Blue: Musculo-tendon-controlled. Red: OpenSim-Simulation.

Using equation 3.4 with a width of 0.6 results in the normalized force-length relation which can be seen in figure 6.5.

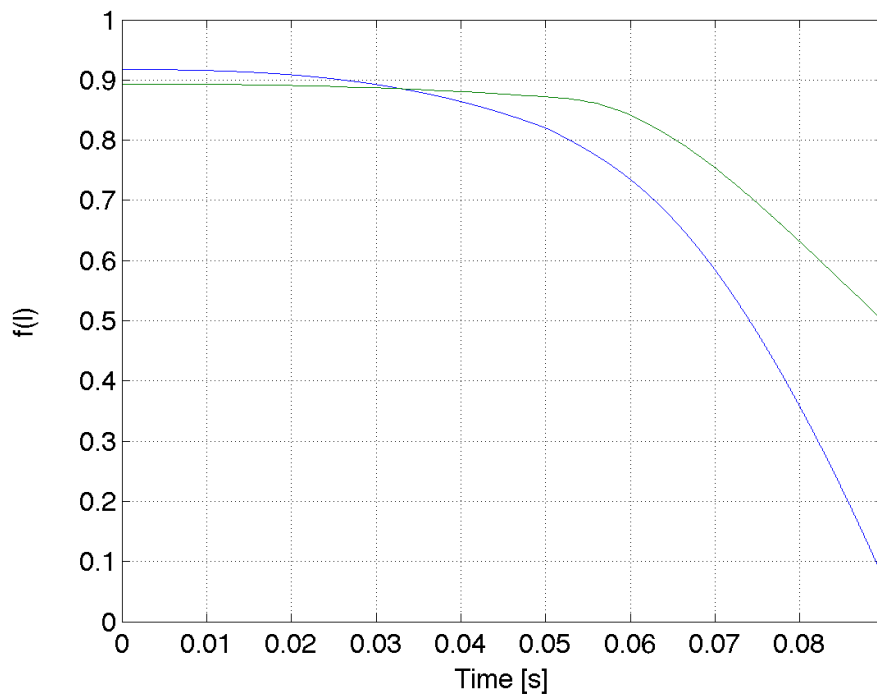


Figure 6.5: Normalized force-length value during ankle movement. Green: Fiber-length-controlled. Blue: Musculo-tendon-controlled.

Figure 6.6 shows the force produced in the fiber over simulation time.

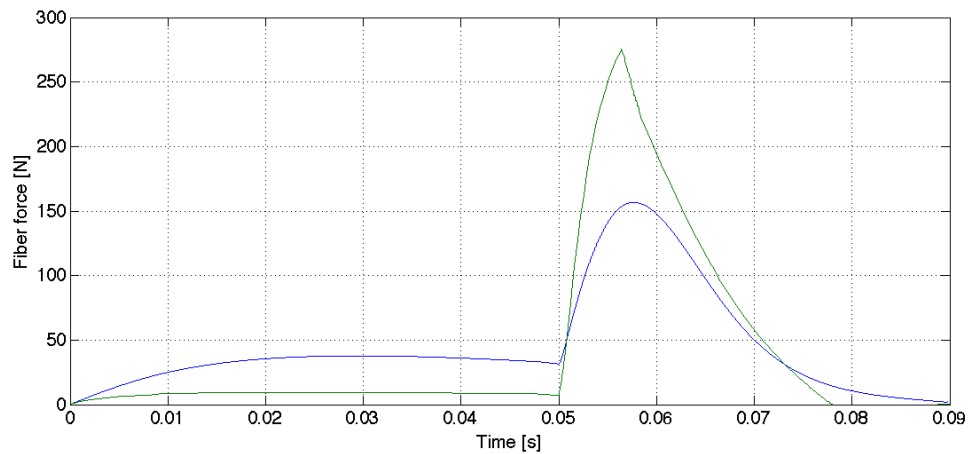


Figure 6.6: Force in the contractile element. Green: Fiber-length-controlled. Blue: Musculo-tendon-controlled.

Figure 6.7 shows the force which acts on the foot through the tendon and causes a plantarflexion.

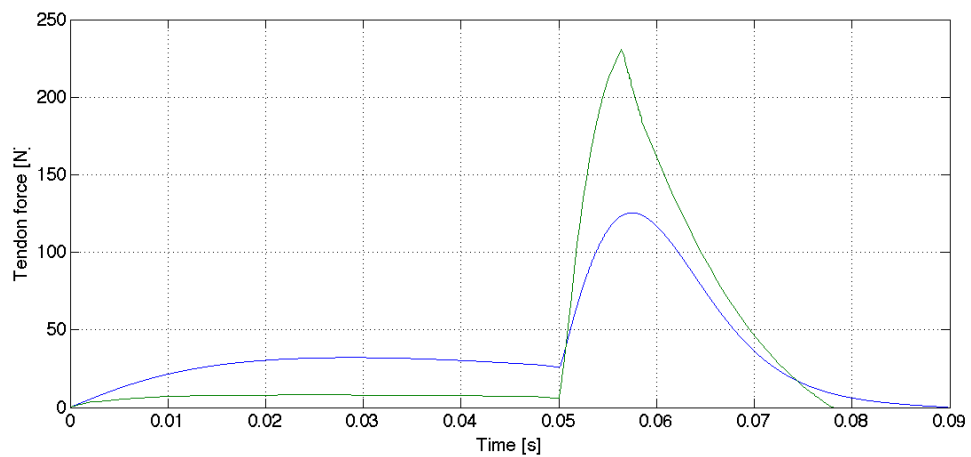


Figure 6.7: Force in the tendon element. Green: Fiber-length-controlled. Blue: Musculo-tendon-controlled.

The ankle movement (plantarflexion) over time for the given excitation (figure 6.1) can be seen in figure 6.8. At 0.05s the stimulation parameter jumps from 0.01 to 1.

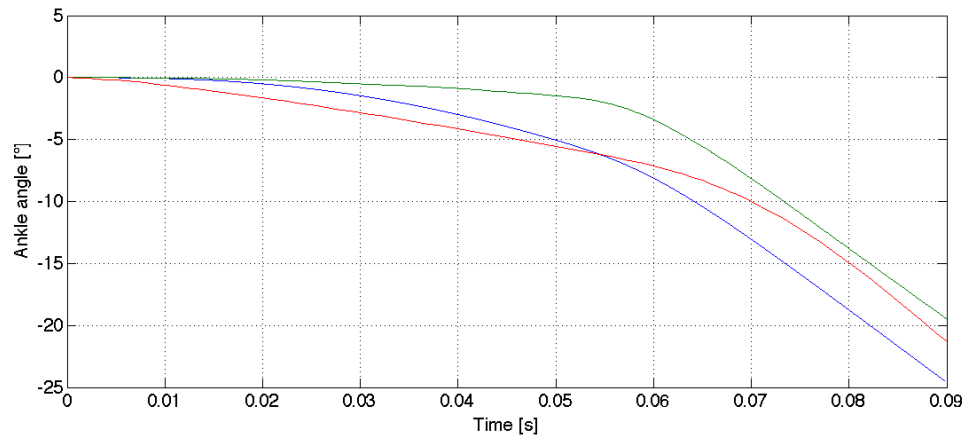


Figure 6.8: Ankle angle over time. Green: Fiber-length-controlled. Blue: Musculo-tendon-controlled. Red: OpenSim-Simulation.

Figure 6.9 shows the difference in the force-length relations of my electrical simulations and the model in OpenSim.

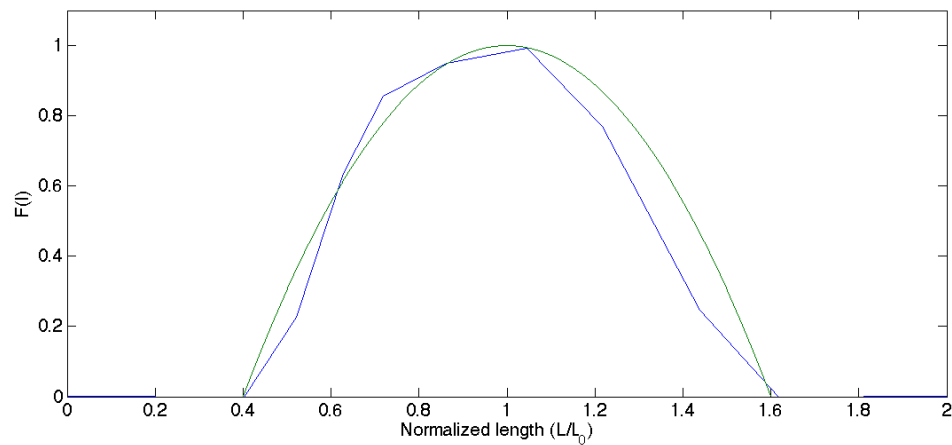


Figure 6.9: Comparison of the different force-length shapes. Green: Force-length shape of GUENTHER [1997]'s equation 3.4. Blue: DLP [1990]'s force-length relation.

## 6.2 Simulation case 2

Three plantarflexor muscles (M. soleus, M. med. gastrocnemius, M. lat. gastrocnemius) and one dorsalflexor (M. tibialis ant.) are innervated with different stimulation signals. The stimulation signals are shown in figure 6.10. The plantarflexors are stimulated with a low signal of 0.02 and the M. tibialis ant. with the maximum signal of 1. The gravity is set to zero. The results of the electrical simulation (only Musculo-tendon-controlled) are compared with an OpenSim-Simulation (3DGaitModel2392).

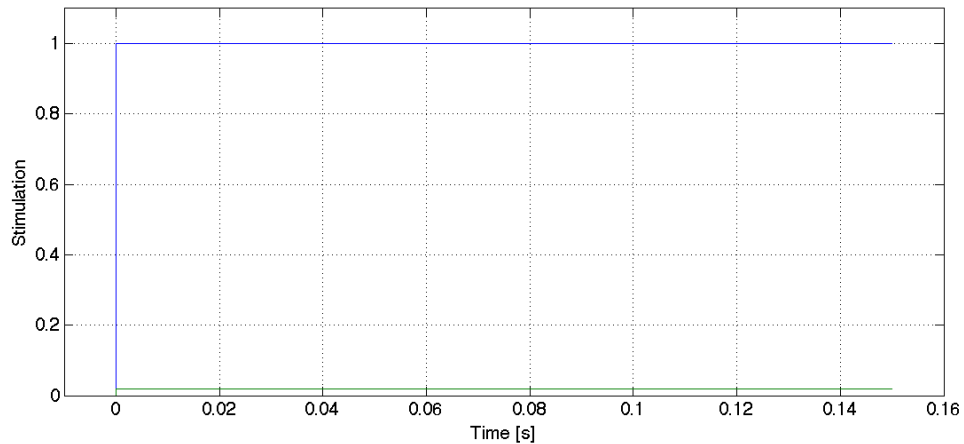


Figure 6.10: Green: Stimulation signal for the three plantarflexors. Blue: Stimulation signal for the M. tibialis ant.

The calculated ankle movement over time can be seen in figure 6.11. The OpenSim-simulation shows a small negative ankle angle at the beginning and a much higher positive angle after 0.15s simulation time.

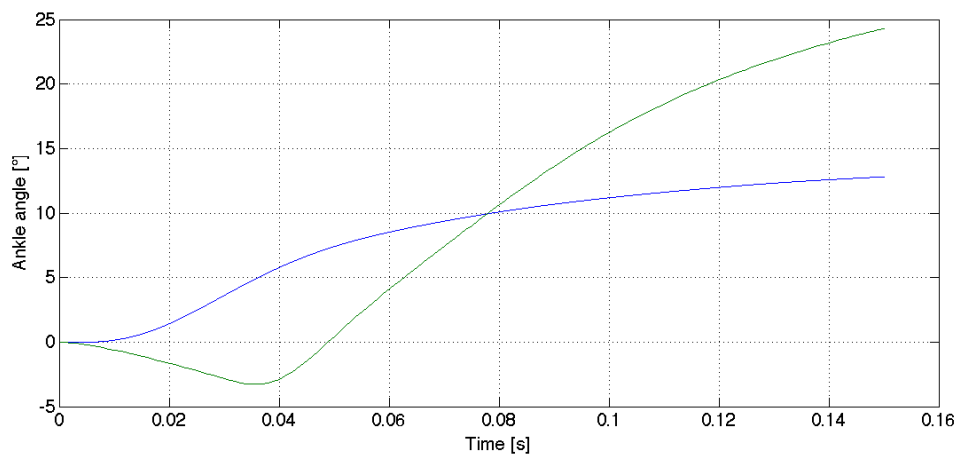


Figure 6.11: Ankle angle over time. Green: OpenSim-Simulation. Blue: Electrical simulation.

Figure 6.12 shows the length of the four stimulated muscles. Because of the positive ankle angle the three plantarflexors elements are stretched and the M. tibialis anterior contractile element is shortened over time. For comparison figure 6.13 shows the fiber length of the muscles during a

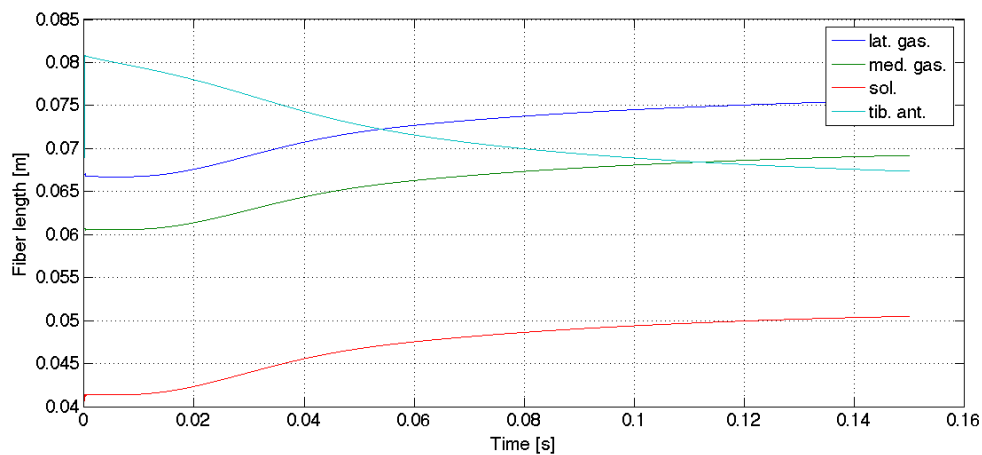


Figure 6.12: Length of the contractile elements of the four stimulated muscles over time in electrical simulation.

simulation with OpenSim. In the 3DGaitModel2392 the fiber lengths are set to a default value: 0.1m for M. med. gastrocnemius, M. lat. gastrocnemius and M. tibialis ant. The default value for the M. soleus is 0.0402m. Due to the negative angle in the first 0.05s the plantarflexors fiber lengths shorten at the beginning. The positive ankle angle causes them to lengthen.

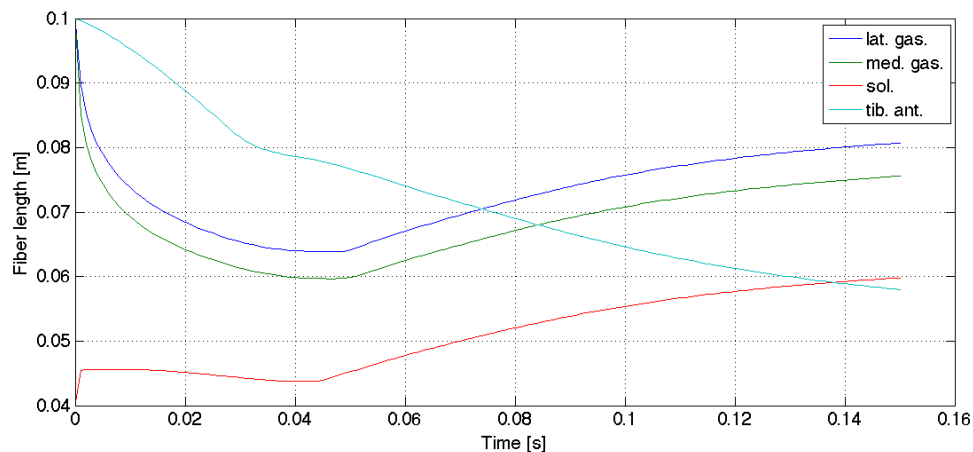


Figure 6.13: Length of the contractile elements of the four stimulated muscles over time simulated with OpenSim.

Figure 6.14 shows the normalized values of the fiber length (figure 6.12). The corresponding optimal fiber length for each muscle can be looked up in table 3.2.

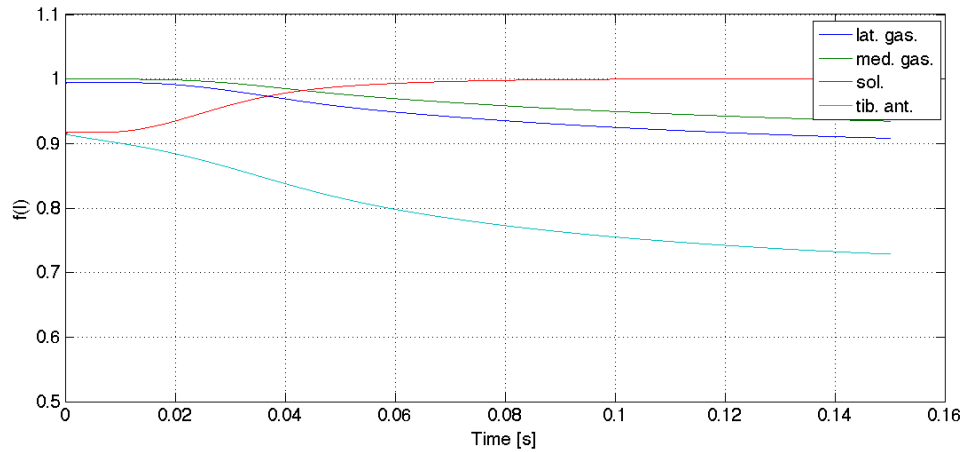


Figure 6.14: Normalized force-length value during ankle movement.

Figure 6.15 shows the contraction velocity of the muscle fibers. Positive values show elongation and therefore eccentric contraction. Negative values indicate a shortening fiber or a concentric contraction. The M. tibialis ant. is contracting concentrically while the plantarflexors perform an eccentric contraction.

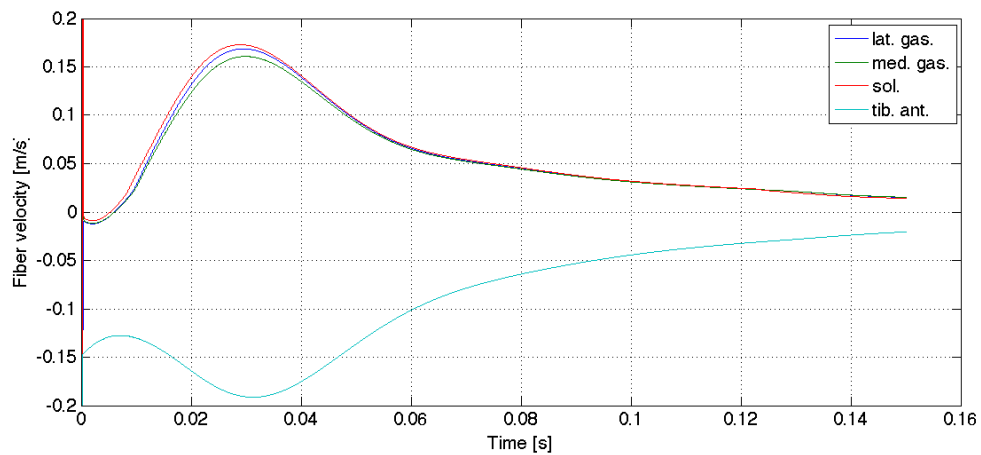


Figure 6.15: Contraction velocity in the contractile elements.

The normalized passive force of the contractile element is shown in figure 6.16. During simulation only M. tibialis ant. shows no passive force because it operates all the time on the shortening side of the force length curve.

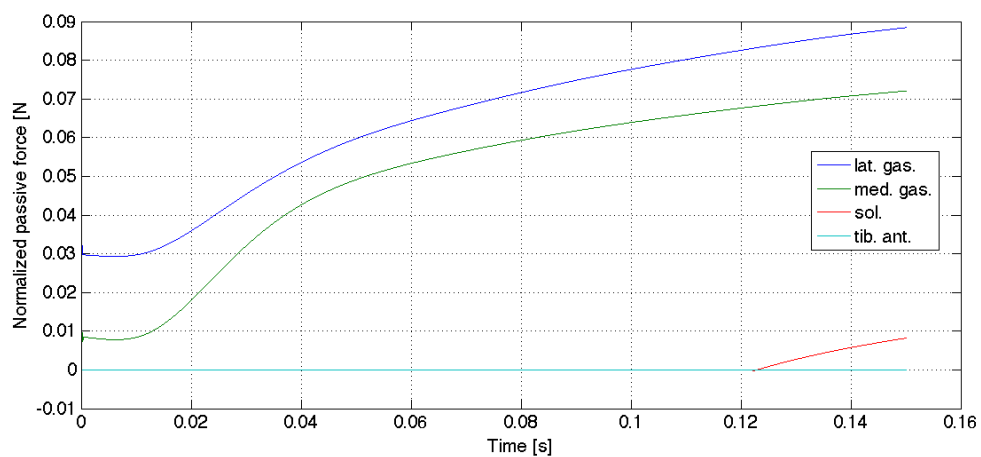


Figure 6.16: Passive force in the contractile elements.

The fiber force of the contractile elements is shown in figure 6.17. The corresponding tendon forces in the next figure 6.18. The different values are due to the multiplication with the pennation angle.

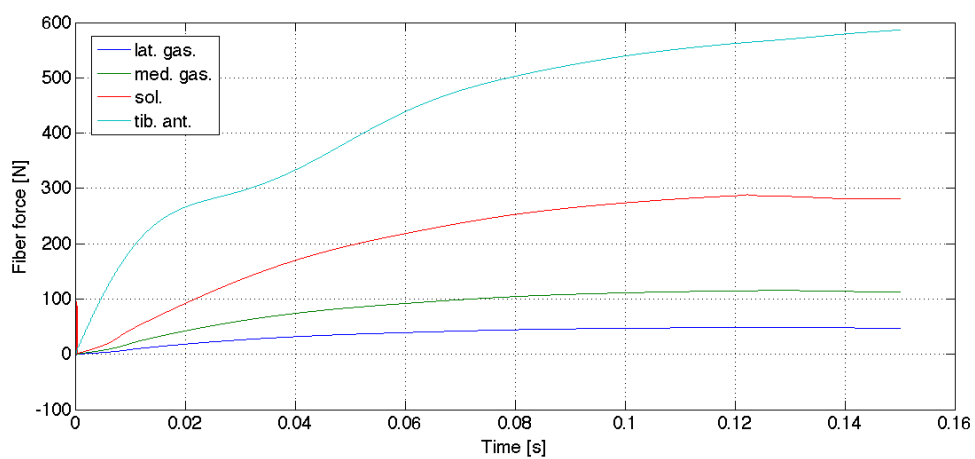


Figure 6.17: Active force in the contractile elements.

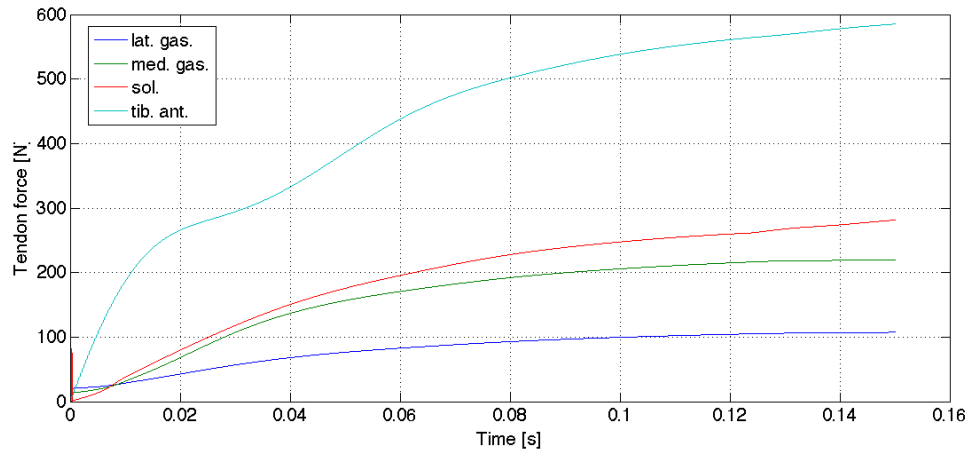


Figure 6.18: Force in the tendons.

The multiplication of the tendon forces with the moment arms results in the joint moments shown in figure 6.19. The resulting moment of the M. tibialis ant. is higher than the accumulated moments of the three plantarflexors. As a result the ankle performs a dorsalflexion. After 150ms simulation time the joint moment produced by M. med. and M. lat. gastrocnemius stays constant. Only M. soleus and M. tibialis ant. still change their produced ankle moment. As a result during simulation time no equilibrium condition is reached.

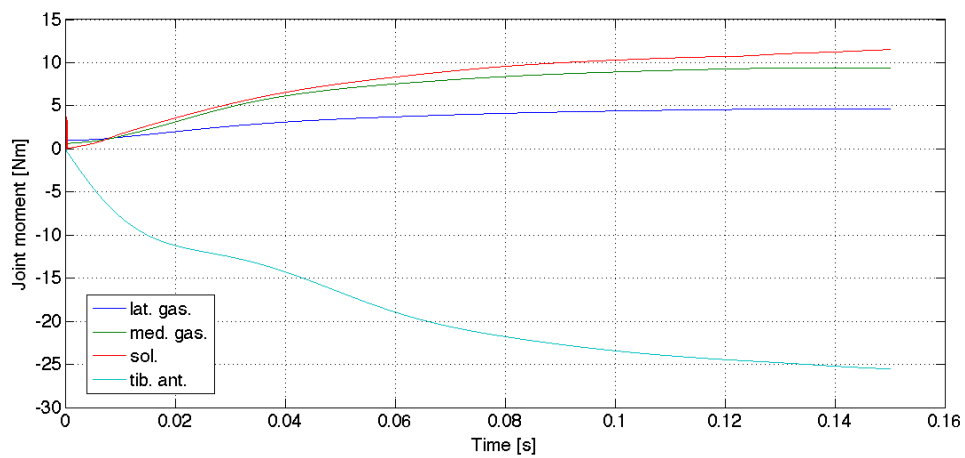


Figure 6.19: Joint moments over time.

## 7 Discussion

### 7.1 Simulation case 1

The stimulation signal for simulation case one is shown in figure 6.1. In the same figure the actual muscle activation is also plotted. Comparing the activation of the electrical stimulation and that of the OpenSim-simulation shows no difference. Both models use the same activation differential equation from ZAJAC [1989]. Also between the two control mechanisms no difference is possible - all simulations were done with the same activation function.

Looking at the pennation angle in figure 6.2 shows that the musculo-tendon-controlled model reaches the  $90^\circ$  pennation angle earlier. The reason for that is the shorter fiber length (figure 6.4). Equation 3.21 calculates the pennation angle with the current fiber length. A pennation angle of  $90^\circ$  is not realistic in my opinion. The  $\cos(\alpha)$  is 0 for  $90^\circ$  and further the equations computing the fiber force are not solvable anymore. Looking at figure 6.5 shows in the musculo-tendon-controlled model that the normalized fiber length becomes nearly 0 when the pennation angle reaches  $90^\circ$ . As a result the force production has to be 0.

The tendon length (figure 6.3) shows values close to the tendon slack length in the musculo-tendon-controlled model. This is much more realistic in comparison to the fiber length controlled model where the fiber has a length of 25.7cm. This results in a strain of 2.8% although the tendon force is not even close to the maximum force  $F_0$ . According to ZAJAC [1989] the tendon force equals the maximum isometric force  $F_0$  when the strain reaches 3.3%. The reason for this tendon length value is the calculation of tendon length in the fiber length controlled model: the tendon length was computed with the data from the OpenSim model 2392 - relating the tendon length to the joint angle. This data from ARNOLD et al. [2010] is only true for isometric muscle contractions.

The fiber length plot (figure 6.4) shows a jump in the OpenSim simulation at the beginning from 0.04m to 0.045m. The reason for that is a default value set to 0.04m at the beginning of every simulation. Over time the shape of the curve looks very similar to that of the musculo-tendon-controlled model. The start value of the fiber length is computed via the start value of the tendon force (equation 5.3). In my simulations the start value of the normalized tendon force was set close to zero (0.01). A force of 0.0 would cause no moment and no change in fiber length or tendon length. As a result the system does not start to swing. In the OpenSim-simulation the default activation value is set to 0.02 to guarantee a moment production. The normalized force-length values in figure 6.5 have the same shape in both control mechanisms as the fiber length plots.

The reason for that is the same equation 3.4 used to compute the normalized force-length values. The computed fiber forces (shown in figure 6.6) show a smoother curve in the musculo-tendon controlled model in comparison to the fiber-length-controlled model. The maximum value is higher during the fiber-length-controlled simulation. The gradient is very high at 50ms. The reason is the stimulation jump from 0 to 1. The shape of the curve in the fiber-length-controlled model can be adjusted with the parameters  $A_{rel}$ ,  $B_{rel}$  and  $FactorQ$  in GUENTHER [1997]'s equation 3.10. The fiber forces never come close to the maximum isometric force  $F_0$  because the fiber shortens very fast and the normalized force-length value decreases. The tendon forces in figure 6.7 show the fiber force multiplied with pennation angle  $\cos(\alpha)$ .

Looking at the ankle angle over time in figure 6.8 states a higher plantarflexion at the beginning of the simulation with OpenSim. After 90ms the angle is in between of the two electrical simulations. All three simulations show a similar slope after 70ms. The reason for the higher plantarflexion at the beginning may be the larger fiber length at the beginning of the simulation. This would cause a higher normalized force-length value. Furthermore in the OpenSim model of ARNOLD et al. [2010] a different shape of the force-length-curve is used (figure 6.9). ARNOLD et al. [2010]'s OpenSim model uses the force-length relation of DELP [1990] showing a non symmetric parabola. On the left side of the curve the decrease of the force with muscle fiber shortening is not as high as in the symmetric parabola which was used in the electrical simulations.

## 7.2 Simulation case 2

The second simulation case was only modeled with the musculo-tendon-controlled approach. The reason for that are the important facts gathered with fiber-length-controlled model in simulation case 1: For the fiber-length-controlled mechanism data of fiber-length over joint ankle is needed. This data is usually not available. Some models like 3DGaitModel2392 in OpenSim include this kind of data but the usually available data is the musculo-tendon length. Furthermore the results in simulation case 1 have shown an unrealistic tendon length because the tendon and it's properties are not included in model-control. ZAJAC [1989] stated that the muscle and tendon always have to be modeled as a unit - the musculo-tendon-unit.

Figure 6.10 shows the stimulation signals for the different muscle groups. The three plantarflexors are stimulated with a signal of 0.02 and the single dorsalflexor (M. tibialis ant.) is fully stimulated at signal strength 1. The value 0.02 is used to compare it with an OpenSim simulation (3DGait-Model2392) - the default value of the stimulation is set to 0.02. The muscle activation can be seen in simulation case one (figure 6.1).

The ankle angle over time is shown in figure 6.11. The electrical model shows no plantarflexion at all. In comparison the same simulation with 3DGaitModel2392 shows a negative angle at the beginning. After 0.04s the angle starts to increase with a higher slope than the electrical simulated one. After 150ms simulation time a difference of about  $10^\circ$  exists.

The fiber-length plot (figure 6.12) shows the length of all four muscle-fibers in the electrical simu-

lation. The fiber-length of the plantarflexors is constant at the beginning. After 20ms the length increases while the fiber-length of the M. tibialis ant. decreases from the beginning. To compare the fiber-lengths over time, figure 6.13 shows the fiber-lengths in the OpenSim simulation. At the beginning of the simulation steep slopes occur. The reason for that are default length values (0.04m for the M. soleus and 0.1m for M. lat. gas., M. med. gas. and M. tib. ant.). The fiber-length stays nearly constant for M. soleus in the first 40ms. Normally the fiber-length of M. tibialis ant. should increase when the ankle angle decreases (the ankle performs a plantarflexion) but this is not the case with 3DGaitModel2392. The shape of the curves after 40ms are comparable with the plots in the electrical simulation. The lengths of the plantarflexors increase (eccentric contraction) and the length of the M. tibialis ant. decreases (concentric contraction). The higher values for the plantarflexors and the lower value for the dorsalflexor correspond to the higher ankle-angle at the end of the simulation.

Figure 6.14 shows the normalized force-length values for the electrical simulation. The plot shows a decreasing value for the M. tibialis ant. - showing that this muscle acts on the shortening side of the force-length-curve. The eccentric working muscles act on different positions on the force-length-curve. On one hand M. gastrocnemius med. and lat. work on the right side. On the other hand M. soleus shows an increasing value and stays at 1. As a result it acts on the left side at the beginning of simulation. Furthermore it shows that the muscle has optimal fiber length when the ankle angle is over 10° dorsalflexion. This is a result of the musculo-tendon-length data which was adopted from ARNOLD et al. [2010]'s model.

The fiber-velocity in figure 6.15 shows negative values for the plantarflexors and positive values for the dorsalflexor. It indicates again eccentric contractions for the plantarflexors and concentric contraction for the M. tibialis ant. The values for the plantarflexors are nearly the same all over the simulation.

Eccentric contractions have to go hand in hand with a force in the parallel elastic element. Figure 6.16 shows a force in the med. and lat. head of M. gastrocnemius which increases over time. This has to be the case because the muscle acts on the right side of the force-length curve all the time. The dorsalflexor shows no passive force and the force in the M. soleus arises at 120ms simulation time.

The fiber-force is much higher in the M. tibialis ant. than in the plantarflexors (figure 6.17). This is the result of a much higher stimulation. The tendon forces in figure 6.18 are the result of the summed active and passive force multiplied with the  $\cos$  of the pennation angle. The pennation angle changes with the muscle length as discussed for simulation case 1. The small difference between the fiber and tendon force for M. tibialis ant. is referred to a very small pennation angle of 5°. For comparison simulation case 1 shows a large difference between the fiber and tendon force for M. soleus. The reason is a much higher pennation angle of 25°.

The tendon forces multiplied with the moment arms result in the acting joint moments in figure 6.19. The negative moment caused by M. tibialis ant. is higher than the accumulated positive moments from the plantarflexors. As a result the ankle performs a dorsalflexion. An increase of

---

simulation time would either show a continuing dorsalflexion until the maximum angle is reached or end up in an equilibrium state where the total moment is 0.

## 8 Conclusion

This work has proven that muscle models can be calculated with an electrical simulation. Two different types of control mechanisms were used to show up the effects of not taking the tendon properties into considerations - the better option to control a forward dynamic simulation is the combination of muscle and tendon as a musculo-tendon unit. Two simulation cases for the human ankle were carried out to show the potential of the model. It is able to accomplish forward dynamic tasks - with a given EMG stimulation signal as an input the model allows detailed examination of ankle angle, moment generation, muscle forces, tendon forces, fiber lengths, tendon lengths and fiber contraction velocities. LTspice IV (1630 McCarthy Blvd., Milpitas, CA) is a perfect system to accomplish such tasks.

The comparison of the electrical and the OpenSim results do not show a perfect match but the model follows the rules of ZAJAC [1989]'s model, which is commonly used in literature. Additionally to the model of ZAJAC [1989] I showed a control mechanism which refers only to the fiber length as the major input. The computed fiber forces look very similar (more edges and not so smooth as musculo-tendon-controlled) but the tendon which has a major impact on the force acting on the joint is not taken into consideration. Furthermore the input data fiber-length over joint angle is not so common and available. On the other hand musculo-tendon-length is easy to determine and is also available in the literature. Therefore it can be stated that the musculo-tendon-control is the approach which should be used in future simulations.

The results of the OpenSim (3DGaitModel2392) simulation show high slopes for the fiber length at the beginning of simulations. This can result in high velocities and furthermore in high joint moments. My electrical simulations do not show such steps.

The calculation of the moment of inertia does not have to match the moment of inertia which is used in OpenSim 3DGaitModel2392. The exact coordinates of the center of masses used in OpenSim 3DGaitModel2392 could not be found out. A difference in the moment of inertia could also have an effect on calculated ankle angle (figure 6.11). The model simulates only in two dimensions and therefore no results for eversion or inversion are shown. The shown model also does not include any friction in the joint. A rebound should also be implemented when the joint angle reaches the maximum. Furthermore the model does not include the gravity, weight of the muscles, time-dependent visco-elasticity of the tendon and also no damping within the muscle.

The model can be used to perform forward dynamic simulation with a given EMG-stimulation as an input. The easy to understandable block-diagrams in electrical engineering make it very comfortable to perform forward dynamic tasks. In an electrical simulation every voltage or current

can be analyzed. As a result every force, moment, velocity can easily be observed. The muscle model can be used to simulate every muscle which works on the same principle as the human one. The input parameters which have to be determined in advance are the musculo-tendon-length over the joint angle, the moment arm over the joint angle, maximum isometric force of the muscle, optimal fiber-length, pennation angle at optimal fiber length and maximum contraction velocity. The determination of these parameters is a very tough task. Every individual human is different and as a result the values vary in a wide range. For example the maximum isometric force for the medial head of the gastrocnemius varies between  $1300N$  and  $1558N$  in different OpenSim models. Different input parameters have a high impact on the output of the simulation.

In future the model should be used to simulate a horse spine. This would be possible if the parameters of horse's muscles and of course the bones with their center of masses and moments of inertia are known. As a result for example the maximum forces and moments on the vertebrae could be determined.

The major disadvantage of using the electrical simulation is the lack of a visible simulation which is available in OpenSim. Adding a graphical interface to see the movements in a horse's spine would make it possible to show the results also to a none professional group.

## References

- Ankle anatomy, 2013. URL [http://www.eorthopod.com/sites/default/files/images/ankle\\_anatomy\\_bones01.jpg](http://www.eorthopod.com/sites/default/files/images/ankle_anatomy_bones01.jpg).
- E.M. ARNOLD, S.R. WARD, R.L. LIEBER, and S. L. DELP. A model of the lower limb for analysis of human movement. *Annals of Biomedical Engineering*, 38(2):269–279, 2010.
- M. BLIX. Die laenge und die spannung des muskels. *Skand. Arch. Physiol.*, 5:149–206, 1894.
- S. BUCHANAN, D.G. LLOYD, K. MANAL, and T.F. BESIER. Neuromusculoskeletal modelling: Estimation of muscle forces and joint moments and movements from measurements of neural command. *J. Appl. Biomech.*, 20(4):367–395, 2004.
- S. L. DELP. *Surgery simulation: A computer graphics system to analyze and design musculoskeletal reconstructions of the lower limb*. PhD thesis, Stanford University, 1990.
- S. L. DELP, J.P. LOAN, M.G. HOY, F.E. ZAJAC, E.L. TOPP, and J.M. ROSEN. An interactive graphics-based model of the lower extremity to study orthopaedic surgical procedures. *IEEE Trans. Biomed. Eng.*, 37:757–767, 1990.
- K.A.P. EDMAN. The velocity of unloaded shortening and its relation to sarcomere length and isometric force in vertebrate skeletal muscle fibres. *J. Physiol.*, 291(143-159), 1979.
- K.A.P. EDMAN, G. ELZINGA, and M.I.M NOBLE. Enhancement of mechanical performance by stretch during tetanic contractions of vertebrate skeletal muscle fibres. *J. Physiol.*, 281:139–155, 1978.
- M. EPSTEIN and W. HERZOG. *Theoretical Models of Skeletal Muscle*. John Wiley & Sons, 1998.
- J.A. FAULKNER, D.A. JONES, J.M. ROUND, and R.H.T. EDWARDS. Dynamics of energetic processes in human muscle. *Proc. Int. Symp. Exerc. Bioenergetics Gas Exchange*, Milan:81–90, 1980.
- J.A. FAULKNER, D.R. CLAFIN, and K.K. McCULLY. Power output of fast and slow fibers from human skeletal muscles. *Human Kinetic Publishers*, 1986.
- A.M. GORDON, A.F. HUXLEY, and F.J. JULIAN. The variation in isometric tension with sarcomere length in vertebrate muscle fibres. *J. Physiol.*, 184:170–192, 1966.

- G.E. GOSLOW and K.M. VAN DE GRAAF. Hindlimb joint angle changes and action of the primary ankle extensor muscles during posture and locomotion in the striped skunk (*mephitis mephitis*). *J. Zool.*, 197:405–419, 1982.
- H. GRAY. Gray, henry. 1918. anatomy of the human body, 1918. URL <http://www.bartleby.com/107/>.
- M. GUENTHER. *Computersimulationen zur Synthetisierung des muskulär erzeugten menschlichen Gehens unter Verwendung eines biomechanischen Mehrkörpermodells*. PhD thesis, Eberhard-Karls-Universität Tübingen, 1997.
- H. HATZE. A myocybernetic control model of skeletal muscle. *Biological Cybernetics*, 25:103–119, 1977.
- H. HATZE. Myocybernetic control models of skeletal muscle - characteristics and applications. *University of South Africa Press*, Pretoria, 1981.
- W. HERZOG and H.E.D.J. TER KEURS. Force-length relation of in vivo human rectus femoris muscles. *Eur. J. Physiol.*, 411:642–647, 1988.
- W. HERZOG, A.C. GUIMARAES, M.G. ANTON, and K.A. CARTER-ERDMAN. Moment-length realtions of rectus femoris muscles of speed skaters/cyclists and runners. *Med. Sci. Sports Exerc.*, 23:1289–1296, 1991.
- W. HERZOG, T.R. LEONARD, J.M. RENAUD, J. WALLACE, G. CHAKI, and S. BORNEMISZA. Force-length properties and functional demands of cat gastrocnemius, soleus and plantaris muscles. *Journal of Biomechanics*, 25:1329–1335, 1992.
- A.V. HILL. The heat of shortening and the dynamic constants of muscle. *Proc. R. Soc. London Ser. B*, pages 136–195, 1938.
- A.V. HILL. First and last experiments in muscle mechanics. *Cambridge University Press*, 1970.
- A.F. HUXLEY. Muscle structure and theories of contraction. *Prog. Biophys. Chem.*, 7:255–318, 1957.
- B. KATZ. The relation between force and speed in muscular contraction. *J. Physiol.*, 96:45–64, 1939.
- Y. KAWAKAMI, Y. ICHINOSE, and T. FUKUNAGA. Architectural and functional features of human triceps surae muscles during contraction. *J. Appl. Physiol.*, 85:398–404, 1998.
- B. KUMMER. *Biomechanik - Form und Bewegung des Bewegungsapparates [p. 335-376]*. Deutscher-Ärzte-Verlag Köln, 2005.

- A. PEDOTTI, V.V. KRISHNAN, and L. STARK. Optimization of muscle-force sequencing in human locomotion. *Math. Biosci.*, 38:57–76, 1978.
- A. PROCHEL. *Erstellung eines komplexen Muskel-Skelett-Modells zur Berechnung der Druckbelastung in Gelenken bei vorwärtsdynamisch simulierten Bewegungsformen*. PhD thesis, Eberhard-Karls-Universität Tübingen, 2009.
- B.J. RIGBY, N. HIRAI, J.D. SPIKES, and H. EYRING. The mechanical properties of rat tail tendon. *J. Gen. Physiol.*, 43(265-283), 1959.
- U. SCHMITZ. *Untersuchung der funktionellen Struktur und Dickenverteilung des Gelenkknorpels der Trochlea tali*. PhD thesis, Med. Uni. Köln, Köln, 1985.
- S. SCOTT and D.A. WINTER. A comparison of three muscle pennation assumptions and their effect on isometric and isotonic force. *Journal of Biomechanics*, 24:163–167, 1991.
- M. SUST. *Beitrag zum Aufbau einer axiomatischen Theorie der Biomechanik und Beispiele ihrer Anwendung*. PhD thesis, Friedrich-Schiller-Universität, Jena 1987.
- M. SUST, I. EICHHORN, K. MESSERSCHMIDT, and T. WEIß. Definition, messung und anwendung von einschaltfunktionen. *Medizin und Sport*, 31:34–36, 1991.
- SWARTHMORE. Analogous electrical and mechanical systems.
- H.E.D.J. TER KEURS, T. IWAZUMI, and G.H. POLLACK. The sarcomere length-tension relation in skeletal muscle. *J. Gen. Physiol.*, 72:565–592, 1978.
- D.G. THELEN. Adjustment of muscle mechanics model parameters to simulate dynamic contractions in older adults. *Journal of Biomechanical Engineering*, 125:70–77, 2003.
- D.G. THELEN, F.C. ANDERSON, and S. L. DELP. Generating dynamic simulations of movement using computed muscle control. *Journal of Biomechanics*, 36:321–328, 2003.
- A.J. VAN SOEST. *Jumping from structure to control: a simulation of study of explosive movements*. PhD thesis, Vrije Universiteit, Amsterdam, 1992.
- E. WAGEMANS and M. VAN LEEMPUTTE. Some structural parameters of m. gastrocnemius linked in a model. *Proc. 12th Int. Cong. Biomech. Los Angeles*, page 316, 1989.
- S.M. WALKER and G.R. SCHRODT. Segment lengths and thin filament periods in skeletal muscle fibers of the rhesus monkey and the human. *Anatom. Record*, 178:63–81, 1973.
- S.R. WARD, C.M. ENG, L.H. SMALLWOOD, and R.L. LIEBER. Are current measurements of lower extremity muscle architecture accurate? *Clin. Orthop. Related Res.*, 467:1074–1082, 2009.

- W. WEBER and E. WEBER. *Mechanik der menschlichen Gehwerkzeuge*. Fischer Verlag, Goettingen, 1836.
- T.L. WICKIEWICZ, R.R. ROY, P.L. POWELL, and V.R. EDGERTON. Muscle architecture of the human lower limb. *Clin. Orthop. Related Res.*, 179:275–283, 1983.
- R.D. WOITTEZ, P.A. HUIJING, H.B.K. BOOM, and R.H. ROZENDAL. A three dimensional muscle model: A quantified relation between form and function of skeletal muscles. *J. Morphol.*, 182:95–113, 1984.
- F.E. ZAJAC. Muscle and tendon: Properties, models, scaling and application to biomechanics and motor control. *Critical Reviews in Biomedical Engineering*, 17:359–411, 1989.
- P. ZELLER. *Handbuch Fahrzeugakustik - Grundlagen, Auslegung, Berechnung, Versuch*, volume 1. Vieweg+Teubner, 2009.